Effects of Ambient Turbulence on Interleaving at a Baroclinic Front

WILLIAM D. SMYTH

College of Oceanic and Atmospheric Sciences, Oregon State University, Corvallis, Oregon

BARRY RUDDICK

Department of Oceanography, Dalhousie University, Halifax, Nova Scotia, Canada

(Manuscript received 10 June 2009, in final form 10 November 2009)

ABSTRACT

In this paper the authors investigate the action of ambient turbulence on thermohaline interleaving using both theory and numerical calculations in combination with observations from Meddy Sharon and the Faroe Front. The highly simplified models of ambient turbulence used previously are improved upon by allowing turbulent diffusivities of momentum, heat, and salt to depend on background gradients and to evolve as the instability grows.

Previous studies have shown that ambient turbulence, at typical ocean levels, can quench the thermohaline interleaving instability on baroclinic fronts. These findings conflict with the observation that interleaving is common in baroclinic frontal zones despite ambient turbulence. Another challenge to the existing theory comes from numerical experiments showing that the Schmidt number for sheared salt fingers is much smaller than previously assumed. Use of the revised value in an interleaving calculation results in interleaving layers that are both weaker and thinner than those observed. This study aims to resolve those paradoxes.

The authors show that, when turbulence has a Prandtl number greater than unity, turbulent momentum fluxes can compensate for the reduced Schmidt number of salt fingering. Thus, ambient turbulence determines the vertical scale of interleaving. In typical oceanic interleaving structures, the observed property gradients are insufficient to predict interleaving growth at an observable level, even when improved turbulence models are used. The deficiency is small, though: gradients sharper by a few tens of percent are sufficient to support instability. The authors suggest that this is due to the efficiency of interleaving in erasing those property gradients.

A new class of mechanisms for interleaving, driven by flow-dependent fluctuations in turbulent diffusivities, is identified. The underlying mechanism is similar to the well-known Phillips layering instability; however, because of Coriolis effects, it has a well-defined vertical scale and also a tilt angle opposite to that of finger-driven interleaving.

1. Introduction

Thermohaline interleaving is a vital mechanism for lateral mixing across watermass boundaries (e.g., Ruddick and Richards 2003). Interleaving may be generated by a variety of processes, including double diffusion (salt fingering or diffusive convection, separately or in combination; Ruddick and Kerr (2003)), molecular diffusion (e.g., Holyer et al. 1987), differential turbulent diffusion (Hebert 1999), and baroclinic instability (McIntyre 1970; May and Kelley 1997). While interleaving signals are often of large amplitude and therefore demand a nonlinear theoretical treatment (e.g., Walsh and Ruddick 1998; Mueller et al. 2007), linear perturbation theory provides an essential starting point for defining spatial and temporal scales and for identifying the central mechanisms (e.g., Stern 1967; May and Kelley 1997; Walsh and Ruddick 2000; Smyth 2007). Here, we use linear analysis to explore the role of ambient turbulence in interleaving driven by salt fingering (more properly, salt sheets, a planar variant of salt fingering that forms when shear is present; e.g., Linden 1974; Kimura and Smyth 2007). We focus on the importance of the turbulent Prandtl number and show how the variability of turbulent fluxes leads to a new class of interleaving mechanisms related to the layering instability of Phillips (1972) and Posmentier (1977).

Corresponding author address: William Smyth, College of Oceanic and Atmospheric Sciences, Oregon State University, Corvallis, OR 97331.
E-mail: smyth@coas.oregonstate.edu

DOI: 10.1175/2009JPO4297.1

This study was motivated by several intriguing discrepancies between theory and observations of thermohaline interleaving. The first discrepancy concerns the suppression of interleaving instability by ambient turbulence. Zhurbas et al. (1988), Kuzmina and Rodionov (1992), and Kuzmina and Zhurbas (2000) analyzed baroclinic fronts unstable to salt fingering and found that a finite value of turbulent diffusivity can suppress interleaving completely. In contrast, Walsh and Ruddick's (2000) study of a barotropic front found that instability exists regardless of the strength of ambient turbulence, though its growth rate is reduced. A later study by Zhurbas and Oh (2001) confirmed that turbulence, even at the relatively low levels common in the ocean interior, can completely prevent interleaving on fingering-favorable baroclinic (though not barotropic) fronts. This leaves us with a paradox: interleaving is observed in many baroclinic fronts where theory suggests it should not happen.

The second discrepancy concerns momentum transport by salt sheets. The Schmidt number Sc^d is the ratio of eddy viscosity to saline diffusivity. The first theory of interleaving (Stern 1967) ignored eddy viscosity (i.e., set $\mathrm{Sc}^d = 0$) and found ultraviolet catastrophe: the growth rate of the instability grows monotonically with increasing vertical wavenumber; therefore, there is no preferred vertical scale. Toole and Georgi (1981) added an eddy viscosity to the model and thereby obtained a preferred scale. Ruddick and Hebert (1988) fit the Toole and Georgi (1981) model to interleaving observed on Meddy Sharon and found that a Schmidt number of 40 gave good agreement. Smyth (2007) repeated this fit, taking baroclinicity into account and found a similar result. There is no evidence, however, that salt sheets possess such high Schmidt number; if anything, the reverse is true. Ruddick et al. (1989) pointed out that, because of the high molecular Schmidt number of seawater, salt sheets growing vertically lose momentum much more rapidly than they lose salinity variance; therefore, they transport salt more effectively, that is, $\mathrm{Sc}^d < 1$. This prediction has now been confirmed in both linear stability analyses (Smyth and Kimura 2007) and nonlinear direct simulations (Kimura and Smyth 2007), which indicate that $\mathrm{Sc}^d \sim 0.1$ or less. With Sc^d this small, the growth rate of interleaving is small and the preferred vertical scale is much too small to match observations. This second paradox suggests that some process other than salt fingering must provide the vertical momentum transport that sets the scale of interleaving. Ambient turbulence is an obvious candidate, except that it also has the property of quenching the instability entirely (see paradox 1).

A third discrepancy concerns the relative amplitudes of the temperature and salinity fluctuations that signal interleaving in observational profiles. On baroclinic fronts, these amplitudes are similar (when expressed in terms of buoyancy fluctuations). Theory suggests, however, that the temperature signal should be at least an order of magnitude stronger (Smyth 2007).

We will show that all three discrepancies can be resolved, or at least greatly mitigated, by the inclusion of an improved turbulence model. The main improvement will be a more realistic representation of the turbulent Prandtl number. Even with this improvement, however, we will, in some cases, be left with predicted growth rates too small to account for observations. To better understand this, we will explore the possibility that interleaving can be observed on fronts that are linearly stable, because the effect of interleaving is to reduce the mean gradients. Every instability is a mechanism for an unstable mean flow to relax to a stable state. Every instability therefore results in a temporary state in which the finite-amplitude fluctuations due to instability are evident, but the mean flow obtained by averaging those fluctuations away is stable. For example, Kelvin–Helmholtz instability is known to be a common mechanism for mixing the oceans (e.g., Gregg 1987; Smyth et al. 2001), even though the necessary condition of subcritical Richardson number is rarely observed. The latter fact is largely due to the reduction of gradients (and hence the increase of the Richardson number) by the instability itself. Here, we will see examples where interleaving growth rates computed from observed mean flows are too small to account for the observed instability, but a modest increase in horizontal gradients (i.e., a decrease in the width of the front) results in a much more robust growth rate. We therefore suggest that instability grew at some previous time when the gradients were steeper and that it has since acted to broaden the front.

Most of our analyses will include the common assumption that turbulent diffusivities are spatially uniform. While this simplification can result in useful insights, turbulence in nature is much more complex. In particular, interleaving layers alter the velocity and buoyancy gradients that support turbulence. As a result, they produce fluctuations in the turbulent diffusivities that mirror the spatial structure of the interleaving and can affect the interleaving growth mechanism. Beyond simply modifying thermohaline interleaving, this feedback loop creates an entirely new class of interleaving mechanisms.

In section 2, a linear, normal mode theory is developed to describe perturbations on a broad, baroclinic front in which both salt sheets and turbulence are active. An energy analysis provides a unified framework to describe the diverse mechanisms that have been proposed for interleaving instability. In section 3, we describe two special classes of solutions that are important in the interpretation of later results: reverse diffusion leading to layering

(Phillips 1972; Posmentier 1977) and the turbulence-driven McIntyre mode (Ruddick 1992). As motivation for later analyses, section 4 contains a brief overview of numerical results showing the effect of turbulence for the particular case of interleaving on the lower flank of Meddy Sharon. In general, the theory does not have analytical solutions simple enough to yield insight; therefore, we rely on numerical explorations of particular points in parameter space. In section 5, though, we develop a simplified analytical representation for the stability boundary that allows us to assess and extend the generality of the numerical results.

The main numerical results are given in section 6. We look at two particular cases: the well-known Meddy Sharon (Armi et al. 1989) and the more strongly baroclinic Faroe Front (Hallock 1985). We find that turbulence, rather than suppressing interleaving, can actually be responsible for setting its vertical scale. We test the hypothesis that interleaving layers observed on fronts that appear stable may be the result of an earlier phase of frontal evolution in which gradients were stronger. We show that an extension of the McIntyre (1970) theory of frontal interleaving, which is entirely independent of double diffusion, accounts well for interleaving on the Faroe Front. Finally, we identify a new class of frontal interleaving instabilities driven by fluctuations in turbulent diffusivities.

2. Theory

a. Equations of motion

Motion is assumed to take place on an f plane. Space is measured by the Cartesian coordinates x, y, and z and the corresponding unit vectors $\mathbf{i}$, $\mathbf{j}$, and $\mathbf{k}$, denoting the cross-front, along-front, and vertical directions, respectively.

The fluid is incompressible and is stratified by temperature and salinity such that the Boussinesq approximation applies. The buoyancy is defined by $b = -g(\rho - \rho_0)/\rho_0$, where ρ is the density with characteristic value ρ_0 and g is the acceleration due to gravity. The equation of state is assumed to be linear, so that b is just the sum of thermal and saline contributions:

$$b = b_T + b_S, \tag{1}$$

with positive b_S being fresh and positive b_T being warm.

The resulting equations of motion are

$$\nabla \cdot \mathbf{u} = 0, \tag{2}$$

$$\frac{D\mathbf{u}}{Dt} = -f\mathbf{k} \times \mathbf{u} - \nabla p + b\mathbf{k} + \nu\nabla^2\mathbf{u} + \frac{\partial}{\partial z}\left(A\frac{\partial \mathbf{u}}{\partial z}\right), \quad \text{and} \tag{3}$$

$$\frac{Db_i}{Dt} = \kappa_i\nabla^2 b_i + \frac{\partial}{\partial z}\left(K_i\frac{\partial b_i}{\partial z}\right), \tag{4}$$

in which $\mathbf{u}$ is the velocity vector,

$$\frac{D}{Dt} = \frac{\partial}{\partial t} + \mathbf{u}\cdot\nabla \tag{5}$$

is the material derivative, t is the time, f is the Coriolis parameter, and p is the pressure scaled by ρ_0. The final terms of (3) and (4) represent parameterized mixing processes; their explicit forms will be given later. In (4) the subscript i may indicate either S for salinity or T for temperature. Molecular viscosity is represented by ν, while κ_i is the molecular diffusivity of salinity or temperature.

Many authors have assumed that interleaving on a baroclinic front must be confined to cross-front modes—that is, layers that do not tilt in the along-front direction—and Smyth (2007) has recently demonstrated the truth of this numerically over a wide range of cases. Accordingly, we assume that $\partial/\partial y = 0$. This allows us to rewrite (2) and (3) as

$$\frac{D\omega}{Dt} = f\frac{\partial v}{\partial z} - \frac{\partial b}{\partial x} + \nu\nabla^2\omega - \frac{\partial^2}{\partial x\partial z}\left(A\frac{\partial^2\psi}{\partial x\partial z}\right) - \frac{\partial^2}{\partial z^2}\left(A\frac{\partial^2\psi}{\partial z^2}\right) \quad \text{and} \tag{6}$$

$$\frac{Dv}{Dt} = -fu + \nu\nabla^2 v + \frac{\partial}{\partial z}\left(A\frac{\partial v}{\partial z}\right), \tag{7}$$

where ψ is a streamfunction for the motion in the $x-z$ plane:

$$u = -\frac{\partial\psi}{\partial z}; \quad w = \frac{\partial\psi}{\partial x} \tag{8}$$

and ω is the corresponding along-front vorticity

$$\omega = \frac{\partial u}{\partial z} - \frac{\partial w}{\partial x}. \tag{9}$$

Motions are assumed to take place in a frontal zone of scale sufficiently large that it can be represented locally by uniform property gradients. The fields are then perturbed by a small-amplitude, cross-front disturbance. The buoyancy fields are therefore given by

$$b_i = B_{i,x}x + B_{i,z}z + b_i'(x, z, t), \tag{10}$$

in which $B_{i,x}$ and $B_{i,z}$ are constants, i once again denotes either S or T, and the subscripts x and z represent partial derivatives. The prime denotes the perturbation. The along-front velocity has a background part that varies linearly in x and z:

$$v = V_x x + V_z z + v'(x, z, t), \tag{11}$$

where V_x and V_z are constants. The streamfunction and vorticity are pure perturbations $\psi = \psi'$; $\omega = \omega'$.

The net vertical gradient of the background buoyancy $B_z = B_{Sz} + B_{Tz}$ is equal to the squared buoyancy frequency, commonly written as N^2. In the fingering-favorable case on which we focus here, $B_{Tz} > 0$ and $B_{Sz} < 0$. The net horizontal gradient of the background buoyancy determines the background shear via the thermal wind balance: $fV_z = B_x = B_{Sx} + B_{Tx}$.

Substituting the flow decompositions (10) and (11) into (4), (1), (6), and (7) gives

$$\begin{aligned}
(\partial_t - \psi'_z\partial_x + \psi'_x\partial_z)\omega' &= fv'_z - b'_x + \nu\nabla^2\omega' - (A\psi'_{x,z})_{x,z} - (A\psi'_{z,z})_{z,z},\\
(\partial_t - \psi'_z\partial_x + \psi'_x\partial_z)v' &= V_x\psi'_x - V_z\psi'_x + f\psi'_x + \nu\nabla^2 v' - [A(V_z + v'_z)]_z,\\
(\partial_t - \psi'_z\partial_x + \psi'_x\partial_z)b'_i &= B_{i,x}\psi'_z - B_{i,z}\psi'_x + \kappa_i\nabla^2 b'_i + [K_i(B_{i,z} + b'_{i,z})]_z, \quad \text{and}\\
\omega' &= -\nabla^2\psi'.
\end{aligned} \tag{12}$$

We assume planar intrusions (neglecting the noses), with uniform tilt angle θ that we treat as a free parameter. The advantage of this approach is that the problem reduces to partial differential equations in one variable plus time, and nonlinear advective terms vanish. Accordingly, the coordinate frame is now tilted by the intrusion angle θ, such that χ represents the tilted x coordinate (along intrusion direction) and ζ represents the tilted z coordinate (across intrusion direction). The rotation operator is

$$\begin{pmatrix} \partial/\partial x \\ \partial/\partial z \end{pmatrix} = \begin{pmatrix} C & -S \\ S & C \end{pmatrix} \begin{pmatrix} \partial/\partial\chi \\ \partial/\partial\zeta \end{pmatrix},$$

where $C = \cos(\theta)$ and $S = \sin(\theta)$.

Perturbations vary only in the ζ direction, so that $\partial/\partial\chi = 0$ for perturbation quantities. Background fields depend on both coordinates. The parameterized diffusivities A and K_i will be defined in detail later. For now we note that the parameterizations depend only on the perturbations and on the gradients of the background fields, which are constants; hence, A and K_i, as well as their associated fluxes, do not vary with χ.

In the rotated frame, the equations become

$$\omega'_t = Cfv'_\zeta + Sb'_\zeta + \nu\omega'_{\zeta,\zeta} - C^2(A\psi'_{\zeta,\zeta})_{\zeta,\zeta}, \tag{13}$$

$$v'_t = V_\chi\psi'_\zeta + fC\psi'_\zeta + \nu v'_{\zeta,\zeta} + C[V_z + Cv'_\zeta)]_\zeta, \tag{14}$$

$$b'_{it} = B_{i,\chi}\psi'_\zeta + \kappa_i b'_{i,\zeta,\zeta} + C[K_i(B_{i,z} + Cb'_{i,\zeta})]_\zeta, \quad \text{and} \tag{15}$$

$$\omega' = -\psi'_{\zeta,\zeta}, \tag{16}$$

where the primed variables are perturbations dependent on ζ and t, and partial differentiation is indicated via subscripts.

We next eliminate ψ' by integrating (13) with respect to ζ (there is no constant of integration since periodicity is assumed). The vorticity ω is equal to $\tilde{u}'_\zeta$, where $\tilde{u}' = -\psi'_\zeta$ is the cross-front velocity parallel to the interleaving layers (and perpendicular to v'). We write the result as

$$\tilde{u}'_t = Cfv' + Sb' - F^u_\zeta, \tag{17}$$

$$v'_t = -(V_\chi + Cf)\tilde{u}' - F^v_\zeta, \quad \text{and} \tag{18}$$

$$b'_{it} = -B_{i\chi}\tilde{u}' - F^i_\zeta, \tag{19}$$

where

$$F^u = -\nu\tilde{u}'_\zeta - C^2A\tilde{u}'_\zeta, \tag{20}$$

$$F^v = -\nu v'_\zeta - C^2Av'_\zeta - CAV_z, \quad \text{and} \tag{21}$$

$$F^i = -\kappa_i b'_{i,\zeta} - C^2K_i b'_{i,\zeta} - CK_iB_{i,z}. \tag{22}$$

The coordinate rotation has removed the nonlinear advection terms, so that linearization is only necessary for the parameterized mixing terms. These are now contained within the fluxes F^u, and so on.

b. Parameterized fluxes

In this subsection we describe a simple format for incorporating parameterized small-scale fluxes into the linearized equations of motion. We then discuss explicit parameterizations for double-diffusive and turbulent fluxes.

1) Linearized forms

Here A is a vertical eddy viscosity that represents the combined effects of double-diffusive instability and shear-driven turbulence. We assume that the two eddy viscosities add linearly. Following Walsh and Ruddick (1995), we assume that the double-diffusive contribution

is determined entirely by the density ratio $R_\rho = -b_{\mathrm{Tz}}/b_{\mathrm{Sz}}$. The turbulent eddy viscosity has been taken as constant in previous studies (e.g., Zhurbas and Oh 2001; Smyth 2007). Our goal here is to improve that representation by expressing the turbulent part as a function of the gradient Richardson number $\mathrm{Ri} = b_z/|\mathbf{u}_z|^2$. Accordingly, we write

$$A = A^d(R_\rho) + A^t(\mathrm{Ri}), \tag{23}$$

in which the superscripts d and t indicate the double-diffusive and turbulent parts, respectively.

Like the other variables, A can be written as the sum of a background part and a perturbation:

$$A = \overline{A} + A'. \tag{24}$$

The background part is given by

$$\overline{A} = A^d(\overline{R}_\rho) + A^t(\overline{\mathrm{Ri}}), \tag{25}$$

where $\overline{R}_\rho = -B_{\mathrm{Tz}}/B_{\mathrm{Sz}}$ and $\overline{\mathrm{Ri}} = B_z/V_z^2$. The perturbation is

$$A' = \frac{dA^d}{dR_\rho}R'_\rho + \frac{dA^t}{d\mathrm{Ri}}\mathrm{Ri}'. \tag{26}$$

The derivatives in (26) are evaluated for the background values $R_\rho = \overline{R}_\rho$ and $\mathrm{Ri} = \overline{\mathrm{Ri}}$. The perturbations can be expanded as

$$R'_\rho = C\overline{R}_\rho\left(\frac{b'_{\mathrm{T}\zeta}}{B_{\mathrm{Tz}}} - \frac{b'_{\mathrm{S}\zeta}}{B_{\mathrm{Sz}}}\right) \quad \text{and} \tag{27}$$

$$\mathrm{Ri}' = C\overline{\mathrm{Ri}}\left(\frac{b'_{\mathrm{S}\zeta} + b'_{\mathrm{T}\zeta}}{B_z} - 2\frac{v'_\zeta}{V_z}\right), \tag{28}$$

and are fluctuations in the density ratio and the Richardson number due to the perturbations. Combining (26)–(28), we have

$$A' = \frac{C}{B_z}\left\{2\frac{f}{s_\rho}\overline{\mathrm{Ri}}\frac{dA^t}{d\mathrm{Ri}}v'_\zeta + \left[\frac{dA^d}{dR_\rho}\overline{R}_\rho(\overline{R}_\rho - 1) + \frac{dA^t}{d\mathrm{Ri}}\overline{\mathrm{Ri}}\right]b'_{\mathrm{S}\zeta} + \left[\frac{dA^d}{dR_\rho}(\overline{R}_\rho - 1) + \frac{dA^t}{d\mathrm{Ri}}\overline{\mathrm{Ri}}\right]b'_{\mathrm{T}\zeta}\right\}, \tag{29}$$

where $s_\rho = -B_x/B_z$ is the isopycnal slope.

The representation for A developed in (23)–(29) carries over trivially to the eddy diffusivities; one simply replaces all occurrences of A with K_i. The linearization is completed by substituting the results into (20)–(22) and discarding the products of perturbations. The results can be written as

$$F^u = -K_{\mathrm{UU}}\tilde{u}'_\zeta, \tag{30}$$

$$F^v = -C\overline{A}V_z - K_{\mathrm{VV}}v'_\zeta - s_\rho f^{-1}K_{\mathrm{VS}}b'_{\mathrm{S}\zeta} - s_\rho f^{-1}K_{\mathrm{VT}}b'_{\mathrm{T}\zeta}, \tag{31}$$

$$F^S = -C\overline{K}_S B_{\mathrm{Sz}} - fs_\rho^{-1}K_{\mathrm{SV}}v'_\zeta - K_{\mathrm{SS}}b'_{\mathrm{S}\zeta} - K_{\mathrm{ST}}b'_{\mathrm{T}\zeta}, \quad \text{and} \tag{32}$$

$$F^T = -C\overline{K}_T B_{\mathrm{Tz}} - fs_\rho^{-1}K_{\mathrm{TV}}v'_\zeta - K_{\mathrm{TS}}b'_{\mathrm{S}\zeta} - K_{\mathrm{TT}}b'_{\mathrm{T}\zeta}. \tag{33}$$

The initial terms on the right-hand sides of (31)–(33) are constants and therefore vanish when substituted into (17)–(19). The remaining terms involve effective diffusivities, which are given by:

$$\begin{aligned}
K_{\mathrm{UU}} &= \nu + C^2(\overline{A}^d + \overline{A}^t),\\
K_{\mathrm{VV}} &= \nu + C^2\left(\overline{A}^d + \overline{A}^t - 2\overline{\mathrm{Ri}}\frac{dA^t}{d\mathrm{Ri}}\right),\\
K_{\mathrm{VS}} &= -C^2\left[(\overline{R}_\rho - 1)\overline{R}_\rho\frac{dA^d}{dR_\rho} + \overline{\mathrm{Ri}}\frac{dA^t}{d\mathrm{Ri}}\right],\\
K_{\mathrm{VT}} &= -C^2\left[(\overline{R}_\rho - 1)\frac{dA^d}{dR_\rho} + \overline{\mathrm{Ri}}\frac{dA^t}{d\mathrm{Ri}}\right],\\
K_{\mathrm{SV}} &= -2C^2\frac{\overline{\mathrm{Ri}}}{\overline{R}_\rho - 1}\frac{dK_S^t}{d\mathrm{Ri}},\\
K_{\mathrm{SS}} &= \kappa_S + C^2\left(\overline{K}_S^d + \overline{K}_S^t - \overline{R}_\rho\frac{dK_S^d}{dR_\rho} - \frac{\overline{\mathrm{Ri}}}{\overline{R}_\rho - 1}\frac{dK_S^t}{d\mathrm{Ri}}\right),\\
K_{\mathrm{ST}} &= -C^2\left(\frac{dK_S^d}{dR_\rho} + \frac{\overline{\mathrm{Ri}}}{\overline{R}_\rho - 1}\frac{dK_S^t}{d\mathrm{Ri}}\right),\\
K_{\mathrm{TV}} &= 2C^2\frac{\overline{\mathrm{Ri}}\,\overline{R}_\rho}{\overline{R}_\rho - 1}\frac{dK_T^t}{d\mathrm{Ri}},\\
K_{\mathrm{TS}} &= C^2\left[-\overline{\gamma}\overline{K}_S^d + \overline{R}_\rho\frac{d(\gamma K_S^d)}{dR_\rho} + \frac{\overline{\mathrm{Ri}}\,\overline{R}_\rho}{\overline{R}_\rho - 1}\frac{dK_T^t}{d\mathrm{Ri}}\right], \quad \text{and}\\
K_{\mathrm{TT}} &= \kappa_T + C^2\left[\overline{K}_T^t + \frac{d(\gamma K_S^d)}{dR_\rho} + \frac{\overline{\mathrm{Ri}}\,\overline{R}_\rho}{\overline{R}_\rho - 1}\frac{dK_T^t}{d\mathrm{Ri}}\right].
\end{aligned} \tag{34}$$

In the expressions for K_{TS} and K_{TT}, we have made the substitution $K_T^d = \gamma K_S^d/R_\rho$, where γ is the flux ratio (defined as minus the ratio of saline to thermal buoyancy fluxes) for salt fingering (e.g., Stern 1967; Walsh and Ruddick 1995).

The signs of the "diagonal" diffusivities K_{UU}, K_{VV}, K_{SS}, and K_{TT} are of particular interest. On the basis of common experience, we expect these to be positive, and

hence to lead to the dissipation of fluctuation variance. This is clearly the case with K_{UU}; however, K_{VV} contains a derivative term that in principle can have either sign. This term originates in the modification of the baroclinic shear by fluctuations in the along-front velocity. These fluctuations locally alter the Richardson number, an effect that shows up here in the effective eddy viscosity. In the vast majority of cases, however, the eddy viscosity A^t decreases with increasing Richardson number, so this effect only makes K_{VV} more positive.

The situation is less simple for the scalar diffusivities. In K_{SS}, the third term in the parentheses involves the derivative of the saline diffusivity of salt sheets with respect to $\overline{R}_\rho$, which is generally negative; hence, the term is positive. The fourth term in parentheses can be negative in diffusive convection ($0 < \overline{R}_\rho < 1$), or in doubly stable stratification ($\overline{R}_\rho < 0$), but it is positive in fingering-favorable stratification ($\overline{R}_\rho > 1$).

In the remainder of this paper, we assume $\overline{R}_\rho > 1$. Therefore, only the thermal diffusivity K_{TT} has a genuine likelihood of being negative in fingering-favorable stratification. The second term in the parentheses can be negative because salt fingering becomes weaker with increasing $\overline{R}_\rho$, and both γ and K_S^d tend to decrease. This leads to a reverse diffusion of thermal gradients in double-diffusive fluids and is thought to be the origin of the ubiquitous thermohaline staircases (Radko 2003). The third term offers an alternative mechanism for reverse diffusion driven by turbulence. In either fingering-favorable ($\overline{R}_\rho > 1$) or doubly stable stratification ($\overline{R}_\rho < 0$), this term is negative, provided that the turbulent thermal diffusivity decreases with increasing Ri, the usual situation. Situations in which $K_{TT} < 0$ will arise repeatedly in this study (see section 3a).

2) Explicit forms for double-diffusive fluxes

Fluxes are conveniently parameterized using flux-gradient laws. These require that diffusivities for momentum (A) and scalars (K_i) be parameterized in terms of background flow properties. Walsh and Ruddick (1995) employed a simple parameterization for the saline diffusivity of salt fingers:

$$K_S^d = K_{S0} R_\rho^{-n_f}. \tag{35}$$

When $n_f = 0$, we have the constant diffusivity employed in the earlier theories. To model dependence on background gradients, we use $n_f = 2.1$ and $K_{S0} = 1.0 \times 10^{-4}$ m^2 s^{-1}, which gives a good fit to the direct simulations of Stern et al. (2001). This is also very close to the parameterization used by Zhang et al. (1998) in the oceanic range of R_ρ values and is within about a factor of three of the observational estimates of St. Laurent and Schmitt (1999).

Momentum diffusivity due to salt fingers is represented in terms of a Schmidt number, $A^d = \mathrm{Sc}^d K_S^d$. Dependence of the double-diffusive Schmidt number on background gradients will be modeled using

$$\mathrm{Sc}^d = 0.08 \ln\left(\frac{R_\rho}{R_\rho - 1}\right), \tag{36}$$

an empirical fit to the numerically determined properties of the fastest-growing linear mode (Smyth and Kimura 2007).

The thermal buoyancy flux due to double diffusion is proportional to the saline buoyancy flux via the flux ratio γ (Stern 1967), leading to $K_T^d = \gamma K_S^d / R_\rho$. We use the expression for the fastest-growing mode from the linear theory of salt fingering (Stern 1975):

$$\gamma = R_\rho - [R_\rho(R_\rho - 1)]^{1/2}. \tag{37}$$

3) Explicit forms for turbulent fluxes

Turbulent fluxes of heat, salt, and momentum are all defined using flux-gradient relations. Thermal fluxes are defined in terms of a diffusivity, K_T^t, that varies from 10^{-6} m^2 s^{-1} in the quietest parts of the ocean through 10^{-5} m^2 s^{-1}, the value that typifies the thermocline, to 10^{-3} m^2 s^{-1} in hot spots such as tidal flow over topography. Salt fluxes are also defined in terms of a diffusivity. In mechanically driven turbulence, saline diffusivity is often assumed to equal thermal diffusivity; however, a significant body of research indicates that this is not exactly true (Gargett 2003; Hebert and Ruddick 2003; Jackson and Rehmann 2003; Smyth et al. 2005): in weak turbulence, the diffusivity ratio $\delta = K_S^t / K_T^t$ tends to be less than unity. Finally, momentum fluxes define an eddy viscosity A^t. The turbulent Prandtl number is the ratio of eddy viscosity to thermal diffusivity $\mathrm{Pr}^t = A^t / K_T^t$. Here Pr^t varies from near unity in strong turbulence to much greater values in weak turbulence.

In much of our work here, we will treat K_T^t, δ, and Pr^t as independent parameters and vary them separately over observed ranges. To refine the resulting picture, though, we must recognize that these parameters are not independent. To this end, we make use of the considerable effort that has gone into parameterizing turbulence in terms of the Richardson number $\mathrm{Ri} = N^2/S^2$. If we can express K_T^t, δ, and Pr^t as functions of Ri, then we can eliminate Ri to give $\mathrm{Pr}^t = \mathrm{Pr}^t(K_T^t)$ and $\delta = \delta(K_T^t)$. Parameterizing δ is beyond our scope here, but we will investigate the effects on interleaving instabilities when $\mathrm{Pr}^t = \mathrm{Pr}^t(K_T^t)$.

A number of Ri-dependent parameterizations have been proposed (Pacanowski and Philander 1981; Peters et al. 1988; Large et al. 1994). All suffer the fundamental limitation that Ri, as a dimensionless parameter, cannot provide the length and velocity scales needed to predict the magnitudes of the turbulent diffusivities; those must be obtained empirically and may not be universal. Also, because of its sensitivity to vertical resolution, Ri is difficult to measure in situ and is likely to be overestimated. Nonetheless, there is little doubt that the balance between stratification and shear quantified by Ri is a dominant factor controlling turbulent diffusivities. All models agree that K_T^t decreases with increasing Ri, approaching a background value when $\mathrm{Ri} \gg O(1)$. Likewise, there is general agreement that $\mathrm{Pr}^t \sim O(1)$ for small Ri and increases more or less linearly for $\mathrm{Ri} \gg O(1)$.

The example we will use here follows Peters et al. (1988), who conducted microstructure measurements in and around the Pacific Equatorial Undercurrent. There, the mean state is characterized by Ri ranging from $O(1)$ or less on the flanks of the undercurrent to $O(10^2)$ in the core of the current and in deeper regions. Peters et al. (1988) were able to fit the resulting range of thermal diffusivities with

$$K_T^t = \kappa_b + \kappa_0(1 + 5\mathrm{Ri})^{-2.5}, \tag{38}$$

where $\kappa_b = 1 \times 10^{-6}$ m^2 s^{-1} is the background diffusivity and $\kappa_0 = 5 \times 10^{-4}$ m^2 s^{-1}. This expression obtains for $\mathrm{Ri} > 1.5$; a stronger dependence is found for smaller Ri. For the eddy viscosity, Peters et al. (1988) found

$$A^t = \nu_b + \nu_0(1 + 5\mathrm{Ri})^{-1.5}, \tag{39}$$

where $\nu_b = 2 \times 10^{-5}$ m^2 s^{-1} and $\nu_0 = 5 \times 10^{-4}$ m^2 s^{-1}.

The background turbulent Prandtl number (in the limit $\mathrm{Ri} \to \infty$) is 20. At smaller Ri, the ratio of the Ri-dependent terms gives

$$\mathrm{Pr}^t = 1 + 5\mathrm{Ri}. \tag{40}$$

Similar linear dependence on Ri has been found independently in studies of sheared, stratified turbulence in the atmosphere (e.g., Esau and Grachev 2007) and in theoretical, laboratory, and observational studies of stratified turbulence (summarized in Galperin et al. (2007)). More generally, (39) and (38) combine to give

$$A^t = \nu_b + \nu_0\left(\frac{K_T^t - \kappa_b}{\kappa_0}\right)^{3/5}, \tag{41}$$

from which Pr^t follows immediately.

The quantities $\overline{\mathrm{Ri}}\, dA^t/d\mathrm{Ri}$, $\overline{\mathrm{Ri}}\, dK_T^t/d\mathrm{Ri}$ and $\overline{\mathrm{Ri}}\, dK_S^t/d\mathrm{Ri}$ appearing in (34) can be obtained as functions of K_T^t in similar fashion. Note that all of these quantities are invariant under a rescaling of Ri. The results needed here are therefore independent of the tendency of observational measurements to overestimate Ri, at least insofar as that overestimation is uniform.

c. The normal mode perturbation equations

Solutions are sought in the normal mode form

$$\tilde{u}'(x, z, t) = u_0 \exp(i\mu\zeta + \sigma t). \tag{42}$$

Only the real part is physically relevant. The exponential growth rate σ is in general complex, while μ is a real cross-intrusion wavenumber and u_0 is a complex constant.

Substituting (42) and similar expressions for v', b_S', and b_T' into the linearized Eqs. (17)–(19) with (30)–(34) yields an algebraic eigenvalue problem

$$\sigma \boldsymbol{v} = A\boldsymbol{v}, \tag{43}$$

where

$$\boldsymbol{v} = (u_0 \quad v_0 \quad b_{S0} \quad b_{T0})^{\mathrm{T}} \quad \text{and}$$

$$A = \begin{bmatrix} -\mu^2 K_{\mathrm{UU}} & Cf & S & S \\ -(Cf + V_\chi) & -\mu^2 K_{\mathrm{VV}} & -\mu^2 s_\rho f^{-1} K_{\mathrm{VS}} & -\mu^2 s_\rho f^{-1} K_{\mathrm{VT}} \\ -B_{\mathrm{S}\chi} & -\mu^2 f s_\rho^{-1} K_{\mathrm{SV}} & -\mu^2 K_{\mathrm{SS}} & -\mu^2 K_{\mathrm{ST}} \\ -B_{\mathrm{T}\chi} & -\mu^2 f s_\rho^{-1} K_{\mathrm{TV}} & -\mu^2 K_{\mathrm{TS}} & -\mu^2 K_{\mathrm{TT}} \end{bmatrix}.$$

Parameterized diffusivities such as K_{UU} are given explicitly in section 2b(1). In what follows, we will explore analytical solutions of (43) for the stability boundary $|A| = 0$ as well as numerical solutions for the fastest-growing mode.

d. The energetics of interleaving

The various classes of interleaving motions discussed here all originate as layered buoyancy variance, created by buoyancy flux convergences of different kinds. Here

we describe a general energy budget that allows us to quantify the various flux convergence processes that lead to interleaving. The energy of interleaving can be partitioned into kinetic and potential reservoirs. These reservoirs exchange energy, both with each other and with several external reservoirs.

- Potential energy stored in the background salinity gradient drives salt sheets and resulting buoyancy fluxes. These can vary with changes in the temperature and salinity gradients brought on by interleaving.
- The background (thermal wind) shear can work with Reynolds stresses to exchange kinetic energy with the perturbations.
- Molecular viscosity–dissipation provides a link to internal energy associated with molecular motions.
- Ambient turbulence generates effective viscosity and diffusivity that fluctuate in response to interleaving.

The kinetic energy of interleaving motions is defined as $\langle K\rangle = {}^1\!/_2\langle \tilde{u}'^2 + v'^2\rangle$, where the angle brackets denote a wavelength average. The rotated Eqs. (17), (18), (20), and (21) can be combined to form the evolution equation

$$\langle K\rangle_t = K_1 + K_2 + K_3 + K_4 + K_5, \tag{44}$$

where

$$K_1 = S\langle \tilde{u}'b'\rangle, \tag{45}$$

$$K_2 = -V_\chi\langle \tilde{u}'v'\rangle, \tag{46}$$

$$K_3 = -\nu\langle \tilde{u}_\zeta'^2 + v_\zeta'^2\rangle, \tag{47}$$

$$K_4 = -C^2\overline{A}\langle \tilde{u}_\zeta'^2 + v_\zeta'^2\rangle, \quad \text{and} \tag{48}$$

$$K_5 = CV_z\langle A_\zeta v'\rangle. \tag{49}$$

The terms K_1, K_2, and K_3 represent changes in kinetic energy due to buoyancy fluxes, shear production, and molecular dissipation, respectively. Term K_4, like K_3, is negative definite and describes the conversion of interleaving kinetic energy to turbulent kinetic energy. Term K_5 results from the cross-intrusion viscosity gradient, which works with the thermal wind shear to produce accumulations of along-front velocity and hence create or destroy perturbation kinetic energy.

The viscosity gradient A_ζ appearing in K_5 is the sum of contributions from turbulent and double-diffusive processes, each of which has components driven by buoyancy and velocity perturbations. Using (27) and (28), we write

$$K_5 = K_{5a} + K_{5b} + K_{5c} + K_{5d}, \tag{50}$$

where

$$K_{5a} = -\mu^2C^2V_z\frac{dA_d}{dR_\rho}\overline{R}_\rho\frac{\langle b_T'v'\rangle}{B_{Tz}}, \tag{51}$$

$$K_{5b} = \mu^2C^2V_z\frac{dA_d}{dR_\rho}\overline{R}_\rho\frac{\langle b_S'v'\rangle}{B_{Sz}}, \tag{52}$$

$$K_{5c} = -\mu^2C^2V_z\frac{dA_t}{d\mathrm{Ri}}\overline{\mathrm{Ri}}\frac{\langle b'v'\rangle}{B_z}, \quad \text{and} \tag{53}$$

$$K_{5d} = 2\mu^2C^2\frac{dA_t}{d\mathrm{Ri}}\overline{\mathrm{Ri}}\langle v'^2\rangle. \tag{54}$$

The first two terms, K_{5a} and K_{5b}, represent convergences due to gradients in R_ρ, and hence in double-diffusive viscosity, caused by thermal and saline buoyancy fluctuations, respectively. The latter two terms result from changes in $A^t(\mathrm{Ri})$ due to buoyancy and along-front velocity fluctuations. These processes contribute to the ultraviolet instability described by (72).

We will see that the buoyancy flux term K_1 in (44) and (46) is the main source of kinetic energy for interleaving. That flux may be described as the conversion to kinetic energy of a potential energy proportional to the buoyancy variance

$$\langle P\rangle = \frac{s}{s - s_\rho}\frac{1}{B_z}\frac{\langle b'^2\rangle}{2}. \tag{55}$$

If the interleaving slope lies outside the baroclinic wedge, that is, $\langle P\rangle > 0$, then interleaving motions must do work against gravity to generate buoyancy variance. Within the baroclinic wedge, $\langle P\rangle < 0$, that is, the growth of buoyancy variance reduces the total potential energy of the fluid.

The sign of the potential energy is irrelevant for our discussion, and we avoid that complication by using an equation for the buoyancy variance based on (19), (22), and the flux parameterizations described in section 2b:

$$\left\langle \frac{1}{2}b'^2\right\rangle_t = B_1 + B_2 + B_3 + B_4 + B_5 + B_6, \tag{56}$$

where

$$B_1 = -B_\chi\langle \tilde{u}'b'\rangle, \tag{57}$$

$$B_2 = -C^2(1-\overline{\gamma})\overline{K}_S^d\langle b_\zeta'b_{S\zeta}'\rangle, \tag{58}$$

$$B_3 = -\kappa_T\langle b_\zeta'b_{T\zeta}'\rangle - \kappa_S\langle b_\zeta'b_{S\zeta}'\rangle, \tag{59}$$

$$B_4 = -C^2\overline{K}_T^t\langle b_\zeta'b_{T\zeta}'\rangle - C^2\overline{K}_S^t\langle b_\zeta'b_{S\zeta}'\rangle, \tag{60}$$

$$B_5 = C\langle (B_{\mathrm{Tz}} K^t_{\mathrm{T}\zeta} + B_{\mathrm{Sz}} K^t_{\mathrm{S}\zeta}) b' \rangle, \quad \text{and} \tag{61}$$

$$B_6 = C\langle B_{\mathrm{Sz}} [(1-\gamma) K^d_S]_\zeta b' \rangle. \tag{62}$$

The term B_1 represents the advection of the background buoyancy gradient B_χ by interleaving motions. When multiplied by the factor $s/(s - s_\rho)B_z$ [cf. (55)], it becomes the negative of K_1, the buoyancy flux term in (44), indicating that it represents a transfer between the kinetic and potential energy reservoirs.

The remaining terms are all diffusive in nature but represent very different physical processes.

- Term B_2 represents the growth of buoyancy variance due to salt sheets and hence the classical model of thermohaline interleaving (Stern 1967). Term B_2 is positive when net buoyancy and saline buoyancy perturbations are negatively correlated (i.e., when warm, salty layers have positive buoyancy and vice versa).
- Term B_3 is the sum of two expressions representing the molecular diffusion of buoyancy variance. If $\kappa_S = \kappa_T$, then B_3 is negative definite and represents simple dissipation. In saltwater, however, $\kappa_S \neq \kappa_T$ and B_3 can be positive. In that case B_3 represents interleaving driven by molecular diffusion, as in laboratory experiments (e.g., Holyer et al. 1987). Note that, if one of $\langle b'_\zeta b'_{\mathrm{S}\zeta} \rangle$ and $\langle b'_\zeta b'_{\mathrm{T}\zeta} \rangle$ is negative, then the other must be positive. Given this and the fact that $\kappa_S < \kappa_T$ in seawater, we see that B_3 can be positive only if B_2 is negative, and vice versa; that is, molecular diffusion drives interleaving with slope opposite to that driven by salt sheets.
- Term B_4 describes the analogous diffusion processes driven by turbulence. It is negative definite if $K^t_T = K^t_S$, but it can be positive otherwise and is then the origin of interleaving driven by differential diffusion (Hebert 1999; Merryfield 2002). It is commonly observed that $K^t_S \leq K^t_T$ in ocean turbulence (e.g., Gargett 2003; Smyth et al. 2005); therefore, B_4 can only be positive if B_2 is negative and vice versa. Differential diffusion therefore opposes salt sheets in the creation of interleaving just as does molecular diffusion.
- Term B_5 describes the creation of buoyancy fluctuations by gradients in the turbulent diffusivities. This term merits particular attention as it is the source of a new interleaving instability to be described in section 6e. Using (28), we can expand B_5 into components driven by velocity and buoyancy perturbations:

$$B_5 = B_{5\mathrm{a}} + B_{5\mathrm{b}}, \tag{63}$$

where

$$B_{5\mathrm{a}} = 2C^2 \overline{\mathrm{Ri}} \left(B_{\mathrm{Tz}} \frac{dK^t_T}{d\mathrm{Ri}} + B_{\mathrm{Sz}} \frac{dK^t_S}{d\mathrm{Ri}} \right) \frac{\langle b'_\zeta v'_\zeta \rangle}{V_z} \tag{64}$$

and

$$B_{5\mathrm{b}} = -C^2 \overline{\mathrm{Ri}} \left(B_{\mathrm{Tz}} \frac{dK^t_T}{d\mathrm{Ri}} + B_{\mathrm{Sz}} \frac{dK^t_S}{d\mathrm{Ri}} \right) \frac{\langle b'_\zeta b'_\zeta \rangle}{B_z}. \tag{65}$$

Note that $B_{5\mathrm{b}}$ can be positive definite, particularly if $K^t_T = K^t_S$ or if either B_{Sz} or B_{Tz} is zero and the other is positive (simple stratification). This term drives the layering instability described by Posmentier (1977) and is discussed in section 3a.

- Term B_6 describes the effect of fluctuating diffusivities due to double diffusion. This term is responsible for the double-diffusive layering modes discussed by Walsh and Ruddick (2000), Radko (2003), and later in section 3a. Using (27), B_6 is easily expanded, just as we have done for B_5. We will not do this explicitly as the expansion is not needed here.

For plotting convenience in the present application, the kinetic energy Eq. (44) is normalized by $\langle K \rangle$, so that the left-hand side is just the real growth rate:

$$\sigma_r = \mathrm{Buoy} + \mathrm{Shr} + \mathrm{DissK} + \mathrm{ConvK_{tB}} + \mathrm{ConvK_{tV}} + \mathrm{ConvK}_d. \tag{66}$$

The mnemonic symbols for the partial growth rates on the right-hand side are defined as

$$\begin{aligned} \mathrm{Buoy} &= K_1/\langle K \rangle \\ \mathrm{Shr} &= K_2/\langle K \rangle \\ \mathrm{DissK} &= (K_3 + K_4)/\langle K \rangle \\ \mathrm{ConvK_{tB}} &= K_{5\mathrm{c}}/\langle K \rangle \\ \mathrm{ConvK_{tV}} &= K_{5\mathrm{d}}/\langle K \rangle \\ \mathrm{ConvK}_d &= (K_{5\mathrm{a}} + K_{5\mathrm{b}})/\langle \mathrm{K} \rangle. \end{aligned} \tag{67}$$

Similarly, (56) is normalized by the buoyancy variance to give

$$\sigma_r = \mathrm{Adv} + \mathrm{SS} + \mathrm{DissB} + \mathrm{ConvB_{tB}} + \mathrm{ConvB_{tV}} + \mathrm{ConvB}_d, \tag{68}$$

where

$$\begin{aligned} \mathrm{Adv} &= \frac{B_1}{\left\langle \frac{1}{2} b'^2 \right\rangle} \quad \mathrm{SS} = \frac{B_2}{\left\langle \frac{1}{2} b'^2 \right\rangle} \quad \mathrm{DissB} = \frac{(B_3 + B_4)}{\left\langle \frac{1}{2} b'^2 \right\rangle} \\ \mathrm{ConvB_{tV}} &= \frac{B_{5\mathrm{a}}}{\left\langle \frac{1}{2} b'^2 \right\rangle} \quad \mathrm{ConvB_{tB}} = \frac{B_{5\mathrm{b}}}{\left\langle \frac{1}{2} b'^2 \right\rangle} \\ \mathrm{ConvB}_d &= \frac{B_6}{\left\langle \frac{1}{2} b'^2 \right\rangle}. \end{aligned} \tag{69}$$

3. Special solutions

Before using (43) to investigate the role of turbulence in thermohaline interleaving, we briefly review two special classes of solutions that represent distinct processes. A third nonthermohaline mechanism for interleaving is described in section 6e.

a. Ultraviolet modes

We begin by examining a class of solutions to (43) that exhibit ultraviolet (UV) catastrophe and can result in the formation of steppy profiles (e.g., Phillips 1972; Posmentier 1977) because of the flux convergence mechanism B_5 (65).

In ordinary diffusion, perturbations decay because an increase in buoyancy gradient causes an increase in downgradient buoyancy flux, and the resulting convergences and divergences smooth the perturbations. However, when the diffusivity decreases sufficiently rapidly with increasing Richardson number, an increase in gradient leads to an increase in Richardson number and to a decrease in flux, causing perturbations to grow. Posmentier (1977) showed how this amounts to a diffusion equation for b_z with a negative diffusivity, leading directly to a positive growth rate proportional to μ^2. In the foregoing analyses, this mechanism is evident in the observations that the buoyancy flux convergence B_5 can be positive and the effective thermal diffusivity K_{TT} can be negative.

Ruddick et al. (1989) verified the existence of this instability for stratified turbulence produced by vertically oriented stirring rods, demonstrating that layers form and then subsequently merge by a similar convergence mechanism at low stirring intensities but are not formed at higher stirring intensities. Estimates of the flux-versus-stirring-intensity relationship were consistent with the Philips–Posmentier theory.

This UV catastrophe mechanism also occurs in double diffusion, beginning with Huppert's (1971) discovery that layers in a double-diffusive staircase will merge if the flux ratio is a decreasing function of density ratio. A similar mechanism leads to layer merging in finite-amplitude thermohaline staircases (Walsh and Ruddick 2000). Consideration of the flux-gradient relationship [e.g., (37)] in a purely vertical salt fingering gradient leads to a similar instability: perturbations cause increases (decreases) in salinity gradient, leading to decreases (increases) in density ratio. Since the buoyancy flux is proportional to $(1 - \gamma)$ times the salt flux, the resulting buoyancy flux convergences cause density perturbations to grow, leading to the formation of thermohaline staircases Radko (2003). The common thread in these instabilities is the convergence of diffusive fluxes: perturbations lead to alterations in flux that cause perturbations to grow. In cases of continuous gradients, it is possible to derive a governing equation for perturbations with an effectively negative diffusivity (71), leading to the $\sigma \sim \mu^2$ UV catastrophe. In both the turbulent and double-diffusive cases, layer formation is followed by layer merging under a closely related mechanism, and similar behavior is expected for the more general class of UV instabilities described later.

In the limit of large wavenumber, (43) has solutions only if $\sigma \propto \mu^2$. Setting $\sigma = \sigma_0 \mu^2$ and taking the limit $\mu^2 \to \infty$, we find

$$(\sigma_0 + K_{\mathrm{UU}}) \| \sigma_0 \mathbf{I} + \Gamma \| = 0, \tag{70}$$

where $\mathbf{I}$ is the 3×3 identity matrix, double bars indicate the determinant and

$$\Gamma = \begin{bmatrix} \sigma_0 + K_{\mathrm{VV}} & s_\rho f^{-1} K_{\mathrm{VS}} & s_\rho f^{-1} K_{\mathrm{VT}} \\ f s_\rho^{-1} K_{\mathrm{SV}} & \sigma_0 + K_{\mathrm{SS}} & K_{\mathrm{ST}} \\ f s_\rho^{-1} K_{\mathrm{TV}} & K_{\mathrm{TS}} & \sigma_0 + K_{\mathrm{TT}} \end{bmatrix}.$$

Any real, positive solution for σ_0 represents a UV instability. Given that $K_{\mathrm{UU}} > 0$, the condition for such an instability to exist is

$$\| \Gamma \| < 0. \tag{71}$$

For example, we may assume that all mixing parameters are constant except for γ, which has derivative $\gamma' < 0$ with respect to R_ρ. In that case, the problem simplifies considerably, and σ_0 has values $-K_{\mathrm{UU}}$, $-K_{\mathrm{SS}}$, and $-K_{\mathrm{TT}}$. Here K_{UU} and K_{SS} are positive definite, but K_{TT} is not [see section 2b(1)]. The corresponding eigenvalue is positive [(71) is satisfied] if $K_{\mathrm{TT}} < 0$, that is, if $\kappa_T / C^2 + K_T^t < -\gamma' K_S^d$. Conversely, if the combination of molecular and turbulent thermal diffusivity is enough to overcome the effect of $\gamma' < 0$, then the instability is suppressed. With the parameterizations described in section 2b(3) and UV instability requires that $R_\rho < 1.39$, a condition that is not typical in frontal zones, though it is by no means unheard of. At lower levels of ambient turbulence, the condition on R_ρ is less restrictive: when $K_T^t = 10^{-6}\ \mathrm{m^2\ s^{-1}}$, diffusive instability requires only that $R_\rho < 2.08$, a common circumstance. The growth rate is a maximum with respect to interleaving slope s when $s = 0$, so the gravitational force that drives interleaving is irrelevant. This instability was first described by Walsh and Ruddick (2000). Because it is independent of the processes that drive interleaving, the instability applies equally to baroclinic and barotropic cases. The same instability has been identified by Radko (2003) as the mechanism for the formation of thermohaline staircases.

Turbulent diffusivities can also drive UV modes. For example, suppose that turbulent diffusivities are dominant and double diffusive and molecular diffusivities can be neglected. Suppose further that there is no differential diffusion, that is, $K_S^t = K_T^t$. One then finds solutions with $\sigma_0 > 0$, provided that

$$\mathrm{Pr}^t + \frac{\mathrm{Pr}^t \mathrm{Ri}}{K_T^t}\frac{dK_T^t}{d\mathrm{Ri}} - 2\frac{\mathrm{Ri}}{K_T^t}\frac{dA^t}{d\mathrm{Ri}} - 4\frac{\mathrm{Ri}^2}{K_T^{t2}}\frac{dK_T^t}{d\mathrm{Ri}}\frac{dA^t}{d\mathrm{Ri}} < 0. \tag{72}$$

The Peters et al. (1988) turbulence parameterization described in section 2b(3) satisfies (72) for $\mathrm{Ri} < 3.185$, or for $K_T^t > 1.4 \times 10^{-6}\ \mathrm{m^2\ s^{-1}}$.[1]

b. McIntyre intrusions

McIntyre (1970) described a particular interleaving instability caused directly by molecular diffusivity. This mechanism can also be driven by turbulent diffusivity and was explored as a possible explanation for interleaving on Meddy Sharon (Ruddick 1992). Here we revisit the relevant theory to derive estimates of the space and time scales applicable in the present context.

In (34), we omit the double diffusive and molecular terms, leaving only the turbulent terms, and in those we set all derivatives with respect to Ri to zero. For simplicity we make the small angle approximation $C \approx 1$. The eigenvalue problem (43) now has the characteristic equation

$$(\sigma + k^2)^2[\sigma + (k^2/\mathrm{Pr}^t)] + G(\sigma + k^2) + J[\sigma + (k^2/\mathrm{Pr}^t)] = 0, \tag{73}$$

where $k^2 = \mu^2 A^t$, $G = f^2(1 + V_\chi/f)$ and $J = \mathrm{SB}_\chi$.

In the laminar case $k^2 = 0$ [denoted as the "classical" case by McIntyre (1970)], (73) becomes

$$\sigma^3 + (G + J)\sigma = 0. \tag{74}$$

Positive roots represent inertial instability. There are no positive roots provided that $G + J \geq 0$. This is equivalent to the condition $\mathrm{Ri}^M \geq 1$, where Ri^M is the geostrophic Richardson number modified to include the effect of cross-front shear:

$$\mathrm{Ri}^M = \frac{f^2}{B_z s_\rho^2}\left(1 + \frac{V_x}{f}\right). \tag{75}$$

Henceforth, we assume that the condition $\mathrm{Ri}^M \geq 1$ is satisfied.

When k^2 is nonzero but small in (73), the trivial root of (74), $\sigma = 0$, becomes nonzero and potentially positive. The new solution is

$$\sigma = -\frac{G + J/\mathrm{Pr}^t}{G + J}k^2 + O(k^6), \tag{76}$$

which is positive (for $G + J > 0$) provided that the numerator is negative, or

$$\mathrm{Ri}^M < \frac{(\mathrm{Pr}^t + 1)^2}{4\mathrm{Pr}^t}, \tag{77}$$

as was shown by McIntyre (1970).

Note that the McIntyre mode is an example of a mode that is destabilized by diffusion. In the laminar limit $k = 0$, the mode is in geostrophic equilibrium and thus has zero growth rate. The effect of turbulent diffusion depends on the Prandtl number: if velocity and buoyancy fluctuations diffuse at the same rate, the mode remains near geostrophic equilibrium as it decays. In contrast, if velocity and buoyancy perturbations decay at different rates (i.e., if the turbulent Prandtl number is different from unity), then the geostrophic balance is upset and the mode has the potential to grow. Later, we will see that thermohaline intrusions in the presence of turbulence exhibit a similar property.

For fixed k^2, we can identify the intrusion slope $s = S/C$ that maximizes the growth rate:

$$s = s_\rho\{\mathrm{Ri}^M - [\mathrm{Ri}^M(\mathrm{Ri}^M - 1)]^{1/2}\}. \tag{78}$$

This preferred slope varies monotonically from s_ρ to zero as Ri^M increases from 1 to ∞; that is, the instability is confined to the baroclinic wedge.

To estimate the value of k^2 that maximizes σ, we must account for the $O(k^6)$ terms in (76). The resulting preferred length scale is given by

$$\mu^4 = \frac{k^4}{A^{t2}} = \frac{8}{3}\frac{B_z}{A^{t2}}\frac{s^3}{s_\rho}\frac{(\mathrm{Ri}^M - 1)^2}{\mathrm{Ri}^M}, \tag{79}$$

and the maximum growth rate is

$$\sigma = -\frac{2}{3}\frac{G + J/\mathrm{Pr}^t}{G + J}k^2. \tag{80}$$

All quantities are evaluated using the preferred values for s and k^2 given in (78) and (79), respectively. Combining (79) with (80) shows that the growth rate is independent of the strength of the turbulence. When Ri^M

[1] This characteristic is not unusual. The parameterization used in the *K*-profile parameterization (KPP) code (Large et al. 1994) for turbulence below the mixed layer satisfies (72) for $\mathrm{Ri} < 0.8$, and the recent parameterization of Zaron and Moum (2009) does the same for $\mathrm{Ri} > 0.15$.

is $O(1)$ (but not <1) and turbulent fluxes are dominant, the McIntyre instability can drive intrusions. Later in this paper, we will give evidence that this mechanism is active on the Faroe Front.

4. Overview of results

To motivate the analyses to follow, we now look briefly at some aspects of the effect of ambient turbulence on interleaving, using the lower flank of Meddy Sharon as our example and (43) as our model. These results will be examined further and generalized to other oceanic regimes in later sections of the paper.

We begin by examining the growth rate of the fastest-growing mode (maximized with respect to the modal parameters μ and s) as a function of isopycnal and isohaline slopes. Diffusivities are made uniform by setting the differentiated quantities in (34) to zero. We likewise set V_x to zero; all other parameter values are characteristic of Meddy Sharon (see Table 1). In the first instance (Fig. 1a), neither molecular diffusion nor ambient turbulence is present. The fastest-growing mode is stationary, as is true for all modes reported here. The growth rate is nonnegative throughout the range of isopycnal and isohaline slopes shown, though it drops to zero on the lines $s_{\mathrm{Sm}} = \pm s_\rho(R_\rho - 1)/(1 - \gamma)$ as predicted by May and Kelley (1997). There are two symmetrical regimes of instability. The upper (lower) regime is unstable to interleaving with positive (negative) layer slope. The observed slopes (bullet) are within the unstable regime, so that interleaving instability is predicted.

The addition of molecular viscosity and diffusion (Fig. 1b) restricts the region of instability, raising minimum isohaline slope for any given s_ρ. As in the inviscid case, the observed slopes are within the region of instability; that is, the front is unstable to thermohaline interleaving. We now add weak turbulent diffusion, with thermal diffusivity 1.7×10^{-6} m^2 s^{-1}, 0.1 times the saline diffusivity of salt sheets. The turbulent Prandtl number Pr^t is set to unity. The minimum isohaline slope needed for instability increases beyond the observed slope (Fig. 1c). With these assumptions, the front is expected to be stable.

Raising Pr^t to 20 reduces the minimum isohaline slope, so that the observed value is once again in the unstable range and instability is predicted (Fig. 1d). The growth rate is too small to account for observations, but if the slopes were steeper by, say, a factor of two (smaller bullet), the growth rate would be substantial. It is plausible that, since interleaving began, it has acted to reduce the slopes, leading to the observed regime where predicted growth is very slow. That possibility will be explored further in section 6b.

TABLE 1. Observed environmental and interleaving parameter values pertaining to the lower flank of Meddy Sharon (May and Kelley 2002; Ruddick 1992) and to the Faroe Front (Hallock 1985). Among the three crossings of the Faroe Front, only s_ρ and s_S were measured separately; the others were assumed equal to the mean state given in column 3.

Parameter	Meddy Sharon	Faroe Front mean	Crossing 5	Crossing 2
$10^3 \times s_S$	27	3.0	6.8	19.0
$10^3 \times s_\rho$	3.6	2.4	5.4	17.2
R_ρ	1.9	2.9	←	←
B_z (s^{-2})	7.4×10^{-6}	2×10^{-5}	←	←
F (s^{-1})	7.7×10^{-5}	1.3×10^{-4}	←	←
$2\pi/\mu$ (m)	25 ± 5	25–100	←	←
r	2 ± 1	1.8 ± 0.5	←	←
$s \times 10^3$	5.7 ± 2.5	Unknown	←	←

5. Critical isohaline slope for interleaving instability

The results of the previous subsection suggest that observations of interleaving on the lower flank of Meddy Sharon can be explained in terms of linear instability theory, and that turbulence, while important, needs not quench the instability entirely in realistic conditions. These preliminary results pertain only to this particular parameter set, however. In this section, we will explore a simplified theory that reveals the effects of turbulence in terms of continuous functions of the environmental flow parameters. We will thereby see that the results suggested earlier can be expected to pertain to a wide range of oceanic parameter regimes.

We begin by assuming that interleaving is represented by stationary modes, that is, modes that do not propagate. The stability boundary is therefore obtained by setting σ to zero in (43), hence the determinant $\|A\|$ must vanish (this boundary is not plotted on Fig. 1, but it lies very close to the lowest plotted contour, $\sigma = 10^{-9} \times \mathrm{s}^{-1}$). The condition $\|A\| = 0$ can be written as

$$\frac{K_{\mathrm{UU}}(R_\rho - 1)}{C^2 B_z}\mu^4 = F(s) = A_2 s^2 + A_1 s + A_0, \quad (81)$$

(recall $s = S/C$ is the slope of the interleaving layers). The quantities A_0, A_1, and A_2 are defined later. In the fingering-favorable regime of interest here, $R_\rho > 1$, so the left-hand side is positive definite.

Before proceeding we must attend to a minor detail: the theory to be developed below requires that A_0, A_1, and A_2 be independent of the interleaving slope s. That requirement would be met except that the effective diffusivities defined in (34) contain slope dependence in the factor C^2. That dependence can be removed in two

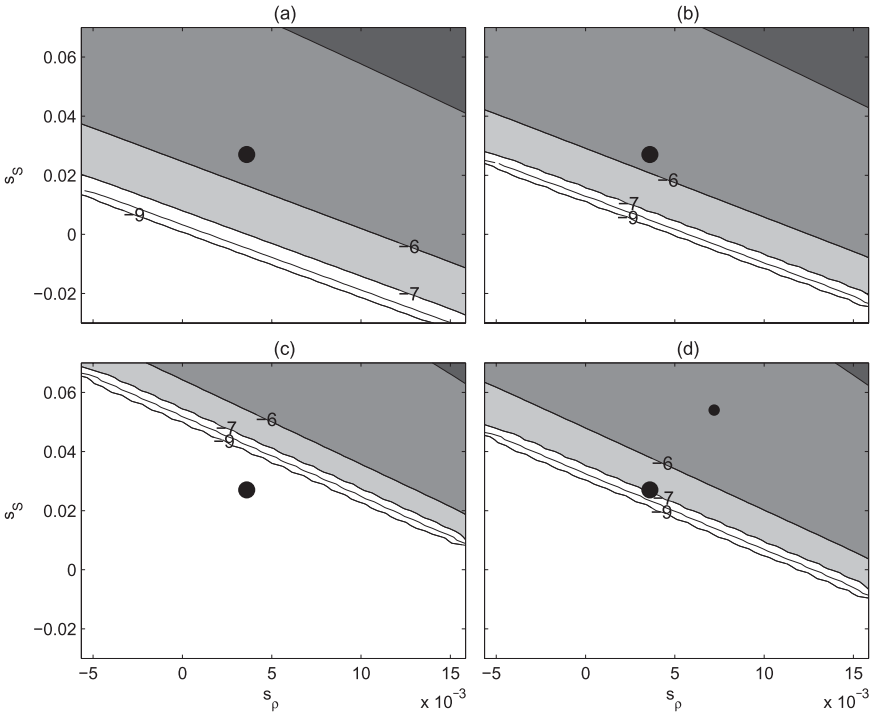

FIG. 1. Common logarithm of the growth rate of the fastest-growing interleaving mode as a function of isohaline and isopycnal slopes. Vertical gradients are characteristic of the lower flank of Meddy Sharon: $N^2 = 7.4 \times 10^{-6}$ s^{-2}, $R_\rho = 1.9$ as is the Coriolis parameter $f = 7.7 \times 10^{-5}$ s^{-1}. Diffusivities due to double diffusion are represented by $K_S^d = 2.6 \times 10^{-5}$ m^2 s^{-1}, Sc$^d = 1$, and $\gamma = 0.59$. Diffusvities are (a) double diffusive only; (b) double diffusive and molecular: $\nu = 10^{-6}$ m^2 s^{-1}, $\kappa_T = 1.4 \times 10^{-7}$ m^2 s^{-1}, $\kappa_S = 1.4 \times 10^{-9}$ m^2 s^{-1}; (c) double diffusive, molecular, and turbulent: $K_T^t = 2.6 \times 10^{-6}$ m^2 s^{-1}, $\delta = 1$, Pr$^t = 1$; and (d) same as (c) except Pr$^t = 20$. All diffusivities are spatially uniform. Large filled circles indicate the isopycnal and isohaline slopes characteristic of the lower flank of Meddy Sharon. For the smaller filled circle in (d), the slopes are doubled.

ways. First, we can make the small-angle approximation $|s| \ll 1$, in which case we replace C^2 by 1 in (34). If we needed to consider large slopes, we could do so at the cost of neglecting the molecular terms ν, κ_S, and κ_T in (34). With that approximation, C^2 becomes a common factor by which (81) can be divided twice. This changes the C^2 in the denominator of the left-hand side to C^6, a change that has no effect on the discussion to follow. Hereafter, we assume that A_0, A_1, and A_2 are independent of s.

In (81), the parabola $F(s)$ opens downward from a vertex at $s = s_0$ provided that $A_2 < 0$. In that case there is, at most, a finite range of slopes in which instability is possible. In the opposite case $A_2 > 0$, instability is always possible for sufficiently large $|s|$. Because interleaving requires finite s, the case $A_2 < 0$ is of primary interest here. In that case, as long as $F(s_0) > 0$, there exists a region of the μ–s plane in which (81) is satisfied, whereas for $F(s_0) < 0$, no such region exists. The condition for instability is therefore $F(s_0) > 0$. This condition can be solved to find s_{Sm}, the minimum value of the isohaline slope needed to drive instability.

The maximum value of $F(s)$ is $F_0 = F(s_0) = A_0 - A_1^2/4A_2$, so that the stability boundary may be written as

$$A_1^2 - 4A_0A_2 = 0. \tag{82}$$

With the previous assumption $A_2 < 0$, nontrivial solutions require that $A_0 < 0$ as well.

In what follows, we focus on the case in which all mixing parameters are uniform; furthermore, we assume that molecular diffusivities are negligible. Both of these assumptions can be relaxed. To simplify the notation, we introduce the nondimensional ratio $\xi = K_T^t/K_S^d$ (following Kuzmina and Zhurbas 2000) and $\tilde{f} = f/\sqrt{B_z}$. We also use the nondimensional quantities δ, Pr^t, and Sc^d, defined previously in section 2b(3).

With the neglect of molecular terms, the effective diffusivities in (34) are proportional to C^2:

$$K_{UU} = K_{VV} = (\mathrm{Sc}^d + \mathrm{Pr}^t\xi)K_S^dC^2$$
$$K_{SS} = (1+\delta\xi)K_S^dC^2$$
$$K_{TS} = -\gamma K_S^dC^2$$
$$K_{TT} = \xi K_S^dC^2$$
$$K_{VS} = K_{VT} = K_{SV} = K_{TV} = K_{ST} = 0, \qquad (83)$$

so we divide that factor out of (81) as discussed earlier. The theory is now valid for arbitrary s.

We next give explicit expressions for the coefficients A_0, A_1, and A_2. We begin by noting that A_1 is a linear function of s_S, that is, $A_1 = A_{10} + A_{11}s_S$, while A_0 and A_2 are independent of s_S. Now,

$$A_0 = -\frac{(R_\rho - 1)(\tilde{f}^2 + s_V s_\rho)}{K_S^d(\mathrm{Sc}^d + \mathrm{Pr}^t\xi)},$$
$$A_{10} = \frac{s_\rho(R_\rho - 1)}{K_S^d}\frac{\mathrm{Sc}^d + \mathrm{Pr}^t\xi + \xi}{\xi(\mathrm{Sc}^d + \mathrm{Pr}^t\xi)},$$
$$A_{11} = \frac{1-\gamma-(1-\delta)\xi}{K_S^d\xi(1+\delta\xi)}, \quad \text{and}$$
$$A_2 = -\frac{R_\rho - \gamma + (R_\rho\delta - 1)\xi}{K_S^d\xi(1+\delta\xi)}. \qquad (84)$$

The condition (82) describing the stability boundary can now be written as a quadratic equation for s_S, whose solution is

$$s_{\mathrm{Sm}} = -S_1 s_\rho \pm S_2(\tilde{f}^2 + s_V s_\rho)^{1/2}, \qquad (85)$$

where

$$S_1 = (R_\rho - 1)\frac{1+\delta\xi}{1-\gamma-\xi(1-\delta)}\frac{\mathrm{Sc}^d + \mathrm{Pr}^t\xi + \xi}{\mathrm{Sc}^d + \mathrm{Pr}^t\xi} \quad \text{and}$$
$$S_2 = \frac{2}{1-\gamma-\xi(1-\delta)}\left\{(R_\rho - 1)\frac{(1+\delta\xi)\xi}{\mathrm{Sc}^d + \mathrm{Pr}^t\xi} \times [R_\rho - \gamma + \xi(R_\rho\delta - 1)]\right\}^{1/2}.$$

Equation (85) is the central result of this section. We will apply it to several important special cases, but first we establish some rules for its proper interpretation. For definiteness we specify the plus sign in (85); this is equivalent to assuming, without loss of generality, that the maximizing slope $s_0 = -A_1/2A_2$ is positive. Note that, when $s_V = 0$ and all other parameters in (85) are fixed, s_{Sm} is a linear function of s_ρ. This linear dependence is evident in the examples shown in Fig. 1.

The isohaline slope specified by (85) is the minimum needed to drive instability, provided that

$$\left.\frac{\partial F_0}{\partial s_S}\right|_{s_S = s_{\mathrm{Sm}}} = s_0 A_{11} > 0. \qquad (86)$$

With the choice of the plus sign in (85), this condition is equivalent to $A_{11} > 0$, or

$$A_{11} = \frac{1-\gamma-(1-\delta)\xi}{K_S^d\xi(1-\delta)} > 0. \qquad (87)$$

Note that $1-\gamma$ and K_S^d are positive in fingering-favorable stratification. In the absence of turbulence, A_{11} is positive and instability requires the isohaline slope to be *larger than* the critical value s_{Sm} given by (85). When $\xi \neq 0$, the result depends crucially on δ. If $\delta > 1$, we once again have $A_{11} > 0$ for arbitrarily strong turbulence. If $\delta < 1$, then $A_{11} > 0$, provided that turbulence is not too strong, more precisely $\xi < (1-\gamma)/(1-\delta)$. If ξ exceeds this limit, then $A_{11} < 0$. In this case, instability occurs when the isohaline slope is *smaller than* s_{Sm}.

Reality of the solution (85) requires that $R_\rho - \gamma + \xi(R_\rho\delta - 1) > 0$. Since $R_\rho - \gamma > 0$ in fingering-favorable stratification and $\xi \geq 0$, we require that either

$$R_\rho\delta - 1 > 0 \quad \text{or} \qquad (88)$$

$$R_\rho\delta - 1 < 0 \quad \text{and} \quad \xi \leq \frac{R_\rho - \gamma}{1 - R_\rho\delta}. \qquad (89)$$

The former condition is expected to be most common. For the latter, $R_\rho\delta < 1$ requires that both R_ρ and δ be at the low end of their observed ranges, that is, very strong double diffusion and very weak turbulence. The accompanying upper limit on ξ is consistent with this scenario. Reality also requires that

$$\tilde{f}^2 + s_V s_\rho > 0, \qquad (90)$$

which is equivalent to the previous assumption $A_0 < 0$.

a. Barotropic nonrotating fronts

Results from several previous studies can be recovered as limiting cases of (85). Consider the barotropic nonrotating case: $s_\rho = \tilde{f} = 0$. In this case, $s_{\mathrm{Sm}} = 0$ regardless of the values of the mixing parameters; that is, any positive isohaline slope is sufficient to drive instability. This is equivalent to the finding that instability persists in the presence of arbitrarily strong ambient turbulence (Walsh and Ruddick 2000).

b. Effects of weak turbulence

We now look at the case where interleaving is driven mainly by double diffusion but is slightly modified by turbulence. Assuming that $\xi \ll 1$ and expanding, we find that

$$s_{\mathrm{Sm}} = -s_\rho \frac{R_\rho - 1}{1-\gamma} + \alpha_0 \xi^{1/2} - s_\rho \alpha_1 \frac{R_\rho - 1}{1-\gamma}\xi + \alpha_0 \alpha_2 \xi^{3/2} + O(\xi^2), \tag{91}$$

where

$$\alpha_0 = 2\left(\frac{\tilde{f}^2 + s_V s_\rho}{\mathrm{Sc}^d}\frac{R_\rho - 1}{1-\gamma}\frac{R_\rho - \gamma}{1-\gamma}\right)^{1/2},$$

$$\alpha_1 = \frac{1}{\mathrm{Sc}^d} + \frac{1-\delta\gamma}{1-\gamma}, \quad \text{and}$$

$$\alpha_2 = \frac{1-\delta}{1-\gamma} + \frac{1}{2}\left(\delta + \frac{1 - R_\rho \delta}{R_\rho - \delta} - \frac{\mathrm{Pr}^t}{\mathrm{Sc}^d}\right).$$

The first term on the right-hand side of (91) gives the minimum isohaline slope for instability in the absence of turbulent (and molecular) diffusivities. This result is implicit in condition (36) of May and Kelley's (1997) analysis of nonturbulent baroclinic fronts.

The second term on the right-hand side is the lowest-order dependence on ambient turbulence. Note first that the turbulence parameters Pr^t and δ do not affect s_{Sm} at this order; that is, the first effect of turbulence on the stability boundary is via the diffusion of temperature anomalies. In fact, the derivative $\partial s_{\mathrm{Sm}}/\partial\xi$ is singular as $\xi \to 0$, so the stability boundary is highly sensitive to the presence of turbulent thermal diffusivity (e.g., Fig. 1c). Because this second term is positive (since $\alpha_0 > 0$), the effect of increasing ξ is to increase s_{Sm}.

The effect is shown schematically in Fig. 2a, arrow 1. For this illustration, we have assumed that s_V is small enough that $\tilde{f}^2 \gg s_V s_\rho$ (or equivalently, $|V_x/f| \ll 1$), so that the stability boundary is a straight line on the s_S–s_ρ plane. In the absence of turbulence, the stability boundary passes through the origin. The lowest-order effect of turbulence is to induce a positive y intercept. This shows that the effect of turbulent thermal diffusion is to damp interleaving modes near the stability boundary, reducing the range of isohaline slopes for which interleaving can grow. This result is a generalization of that shown explicitly in Fig. 1 for the special case of Meddy Sharon. The effect of turbulence on the stability boundary is highly sensitive to the double-diffusive Sc^d and is amplified in the present results because we take $\mathrm{Sc}^d \ll 1$.

This tendency for ambient turbulence to oppose double-diffusive interleaving is consistent with the results of Zhurbas and Oh (2001). Discarding the two higher-order terms, (91) can be solved to estimate the marginal value ξ_{mar} above which instability is quenched for a given s_S:

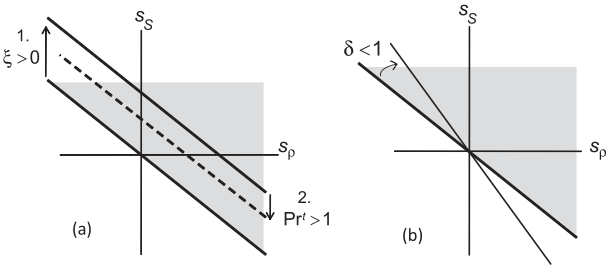

FIG. 2. (a) Schematic showing the lowest-order effects on the stability boundary due to the imposition of weak turbulent thermal diffusivity (arrow 1) and an increase in the turbulent Prandtl number (arrow 2). Shading indicates instability. (b) Differential diffusion (reduction of δ below unity) increases the (negative) slope of the stability boundary.

$$\xi_{\mathrm{mar}} = \frac{\mathrm{Sc}^d}{4\mathrm{Ri}^M}\left(\frac{s_S}{s_\rho}\frac{1-\gamma}{R_\rho - 1} + 1\right)^2 \frac{R_\rho - 1}{R_\rho - \gamma}. \tag{92}$$

This may be compared with the corresponding Eq. (12) of Zhurbas and Oh (2001), where s_ρ was set to zero. If we assume $\xi \ll 1$ in the Zhurbas and Oh result and take the limit $s_\rho \to 0$ in (92), then the results agree. While serving to illustrate the relationship between the present results and those of Zhurbas and Oh (2001), (92) is of limited practical use because the right-hand side is typically not $\ll 1$ as was assumed.

We now go beyond previous studies by looking at the effects of the other two turbulence parameters, Pr^t and δ, which quantify the effects of momentum and salt diffusion (respectively) relative to thermal diffusion. To assess the role of Pr^t, we differentiate the $O(\xi^{3/2})$ term of (91) to obtain

$$\frac{\partial s_{\mathrm{Sm}}}{\partial \mathrm{Pr}^t} = -\frac{\alpha_0}{2\mathrm{Sc}^d}\xi^{3/2}. \tag{93}$$

Since $\alpha_0 > 0$, the right-hand side is negative and the effect of increasing Pr^t in weak turbulence is therefore to expand the region of instability [Fig. 2a, arrow 2; also Fig. 1d].

Note that to increase Pr^t with ξ fixed is to increase the turbulent viscosity, so this is an example of a mode destabilized by diffusive effects similar to the McIntyre mode (section 3a). The dynamic is more complicated: modes on the stability boundary are maintained by a modified geostrophic balance involving double-diffusive fluxes as well as the Coriolis and gravitational forces. The action of turbulent diffusion is the same, though; by diffusing momentum faster than buoyancy, it upsets the equilibrium and allows the mode to grow. Later we will see that turbulence also has important effects on the fastest-growing mode, including destabilization by turbulent viscosity. As

with ξ, the effect of Pr^t on the stability boundary is amplified when Sc^d is small and when Ri^M is large.

Next, we examine the effect of the diffusivity ratio δ on the stability boundary in the weak turbulence limit:

$$\frac{\partial s_{\mathrm{Sm}}}{\partial \delta} = \frac{R_\rho - 1}{1-\gamma}\frac{\gamma}{1-\gamma} s_\rho \xi. \tag{94}$$

Recall that differential diffusion usually involves a *reduction* in δ from unity. Since the derivative has a positive factor multiplying s_ρ, the $O(\xi)$ effect of a reduction in δ is to *increase* the negative slope of the stability boundary, as shown schematically on Fig. 2b. Recall that s is assumed to be positive, so when $s_S > 0$, the interleaving slope is consistent with generation by salt sheets. The effect of differential diffusion is then to stabilize interleaving near the stability boundary. Conversely, if $s_S < 0$, then the interleaving slope is consistent with differential diffusion, and modes near the stability boundary are correspondingly destabilized.

An indirect effect of turbulence occurs via the cross-front shear V_x. In the presence of turbulence (and only then!), nonzero cross-front shear alters the stability boundary. At lowest order in ξ, the effect depends on the sign of s_V. Cross-front shear acts to enlarge the regime of instability if s_V has a sign opposite to s_ρ. Because the product $s_V s_\rho/\tilde{f}^2$ is equal to V_x/f, instability is enhanced if $V_x/f < 0$, that is, if the cross-front shear acts to reduce the absolute (relative plus planetary) vertical vorticity. Conversely, the regime of instability is restricted if V_x is such as to increase absolute vorticity. This result is reminiscent of the stabilization of columnar vortices by increases in absolute vorticity (e.g., Smyth and McWilliams 1998).

c. *Effects of strong turbulence*

Another interesting case is that of interleaving driven primarily by turbulence, accessed via the limit $\xi \to \infty$. To begin with, we will assume $\delta = 1$ and ξ is $\gg 1$. In this case,

$$s_{\mathrm{Sm}} = \xi \frac{2}{\mathrm{Pr}^{t1/2}} \frac{R_\rho - 1}{1-\gamma}\left[(\tilde{f}^2 + s_V s_\rho)^{1/2} - s_\rho \frac{\mathrm{Pr}^t + 1}{2\mathrm{Pr}^{t1/2}}\right]. \tag{95}$$

For the graphical description (Fig. 3), we again assume that $\tilde{f}^2 \gg s_V s_\rho$, so that s_{Sm} is a linear function of s_ρ with negative slope. Its x intercept (shown by a circle) is given by $s_{\mathrm{Sm}} = 0$ and $s_\rho = \bar{s}_\rho$, where

$$\bar{s}_\rho \equiv \frac{2\mathrm{Pr}^{t1/2}}{\mathrm{Pr}^t + 1}(\tilde{f}^2 + s_V s_\rho)^{1/2}. \tag{96}$$

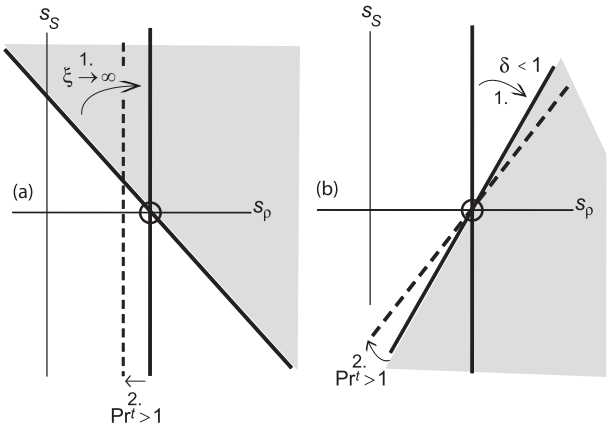

FIG. 3. (a) Schematic for the "strong turbulence" limit, showing the tilting of the stability boundary as $\xi \to \infty$ (arrow 1) and the expansion of the unstable region as the turbulent Prandtl number is increased above unity (arrow 2). (b) Differential diffusion tilts the stability boundary to the right (arrow 1). Tilting is increased when $\mathrm{Pr}^t > 1$ (arrow 2). Circles indicate the critical isopycnal slope $\bar{s}_\rho$.

The region of instability is the half plane above this line. As $\xi \to \infty$, the line rotates clockwise about its x intercept until it becomes vertical (arrow 1 in Fig. 3a). Instability exists only to the right of the line, or when

$$s_\rho > \bar{s}_\rho. \tag{97}$$

This condition describes the McIntyre (1970) instability, since (97) is equivalent to (77) (note that $\tilde{f}^2 + s_V s_\rho = s_\rho^2 \mathrm{Ri}^M$). In section 6c, we will see an example of an observed front where the McIntyre instability may be important. Conversely, the effect of salt sheets, expressed as finite ξ, is to rotate the line counterclockwise away from the vertical. The McIntyre (1970) instability is therefore enhanced by salt sheets when its tilt is consistent with that of salt sheet–driven interleaving ($s_0 > 0 \Rightarrow s_S > 0$).

The effect of increasing Pr^t is to reduce $\bar{s}_\rho$, so that the region of instability expands (arrow 2 in Fig. 3a). Because of the factor $\mathrm{Pr}^{t1/2}$ in the denominator of (95), increasing Pr^t above unity also slows the rate at which the line approaches the vertical as $\xi \to \infty$. When s_V is not small, (96) and (97) remain true, but the "line" we have referred to acquires a nonzero curvature. This complicates the graphical interpretation but does not alter the essential results.

Suppose now that the ambient turbulence exhibits differential diffusion with $\delta < 1$. In this case, $\partial F_0/\partial s_S|_{s_S = s_{\mathrm{Sm}}} < 0$ [recall (86, 87) and the accompanying discussion], so that s_{Sm} now represents a *maximum* isohaline slope *below* which the mean state is unstable. That maximum slope is given by

$$s_{\mathrm{Sm}} = -\frac{2\delta}{1-\delta}\frac{R_\rho - 1}{\mathrm{Pr}^{t1/2}} \times \left[(\tilde{f}^2 + s_V s_\rho)^{1/2}\left(\frac{R_\rho - 1/\delta}{R_\rho - 1}\right)^{1/2} - s_\rho \frac{\mathrm{Pr}^t + 1}{2\mathrm{Pr}^{t1/2}}\right]. \quad (98)$$

The maximum isohaline slope is now independent of ξ, but it depends crucially on δ, especially when the latter is close to unity. We will consider the limit of weak differential diffusion, defined as $\delta \to 1^-$. In this case,

$$s_{\mathrm{Sm}} = -\frac{2}{1-\delta}\frac{R_\rho - 1}{\mathrm{Pr}^{t1/2}}\left[(\tilde{f}^2 + s_V s_\rho)^{1/2} - s_\rho \frac{\mathrm{Pr}^t + 1}{2\mathrm{Pr}^{t1/2}}\right]. \quad (99)$$

Note the similarity to (95). In this case, s_{Sm} is a linear function of s_ρ with *positive* slope, and instability is found for values below this line (Fig. 3b). The x intercept is the same as in the previous case: $s_\rho = \bar{s}_\rho$. Weak differential diffusion ($\delta < 1$) modifies the McIntyre instability, such that the stability boundary rotates clockwise from the vertical. Instability is then favored [i.e. the condition (97) is relaxed] when $s_S < 0$; that is, the slopes are consistent with interleaving due to differential diffusion. The rotation of the stability boundary away from the vertical due to differential diffusion is enhanced when $\mathrm{Pr}^t > 1$ because of the factor $\mathrm{Pr}^{t1/2}$ in the denominator of (99) (arrow 2 in Fig. 3b). Increasing Pr^t also reduces $\bar{s}_\rho$, as in the $\delta = 1$ case (Fig. 3a in arrow 2). Conversely, in the regime of interleaving due to salt sheets $s_S > 0$, modes near the stability boundary are stabilized by differential diffusion.

Recall that the cross-front velocity affects the stability boundary only in the presence of turbulence. As in the weak turbulence limit, the regime of instability in the presence of strong turbulence is expanded (contracted) when $V_x/f < 0$ (>0).

d. Effects of molecular diffusion

The theory for interleaving driven by the molecular diffusion was explored by Holyer (1983). In the small angle limit $C^2 \to 1$, the molecular diffusivities ν, κ_T, and κ_S appear simply as constants added to the corresponding turbulent diffusivities A^t, K_T^t, and K_S^t. The effects on the critical isohaline slope are therefore identical to those of turbulence with constant diffusivity as described earlier. Most importantly, weak molecular diffusivity reduces the region of instability by diffusing temperature anomalies, as does weak turbulence. Turbulence is more likely to play a significant role in interleaving—first, because its diffusivities are generally stronger, and second, because its Prandtl number is higher, so that significant momentum can be diffused without diffusing away the thermal anomalies that drive the instability.

e. Summary

Both the weak and strong turbulence regimes reveal the following effects of turbulence on thermohaline interleaving:

- Adding turbulent diffusivity ξ reduces the regime of instability, except when baroclinicity is strong enough to support the McIntyre (1970) mechanism.
- Increasing Pr^t expands the region of instability. This leads to the counterintuitive conclusion that an increase in eddy viscosity *destabilizes* interleaving modes, as long as it is not accompanied by an increase in thermal diffusivity. The explanation appears to lie in the ability of different diffusivities to upset balances (e.g., thermal wind) that otherwise restrain growth.
- Differential diffusion acts in opposition to salt sheets, driving interleaving with opposite slope. It therefore expands (contracts) the regime of instability where $ss_S < 0$ (>0).

The first two of these effects are evident in the illustrative examples discussed in section 4.

This section has focused on modes close to stability boundaries. Such modes typically grow too slowly to be important and are quickly overtaken by the fastest-growing mode. Nevertheless, changes in the stability boundary are often reflected in changes in the fastest-growing mode. In a stratified shear layer, for example, increasing stratification both dampens the fastest-growing mode and contracts the range of wavenumbers over which instability is possible (Hazel 1972). Since analytical results for the fastest-growing mode are not available, we have used changes in the stability boundary as a first indication of its behavior. In the following section, we will examine the fastest-growing mode directly via numerical solutions for specific cases, and we will see several examples in which the relationships suggested in the present section are in fact valid.

6. Effects of turbulence on the fastest-growing mode: Comparison with observations from two oceanic fronts

Here we test the ability of the theory described earlier to predict interleaving across observed fronts. As input, the theory requires values for the environmental parameters f, B_z, R_ρ, s_S, and s_ρ as well as the parameters appearing in the mixing models. The front separating Meddy Sharon from the surrounding ocean was surveyed in detail (Armi et al. 1989), and the needed parameter values have been summarized conveniently by May and Kelley (2002). Those values are listed in the second column of Table 1. The Faroe Front was measured in five

transects reported by Hallock (1985). Hallock published sections of temperature and density for two individual transects as well as the average of all five, and the needed environmental parameters can therefore be estimated (columns 3–5 of Table 1). These differ from the Meddy Sharon case in that baroclinicity is more pronounced; the isopycnal slope is nearly as steep as the isohaline slope. Not surprisingly, the averaged section yields relatively gentle slopes, whereas the individual transects exhibit steeper slopes.

Measurable interleaving parameters that the theory can predict include the following:

- the vertical scale of interleaving $2\pi/\mu$,
- the amplitude ratio $r = \max_z|b'_T|/\max_z|b'_S|$, and
- the slope s.

The vertical scale and the amplitude ratio are easily extracted from vertical profiles of temperature and salinity. We note that the predicted vertical scale $2\pi/\mu$ may be a lower bound if subharmonic instabilities are present. Such modes are evident in simulations of interleaving driven by diffusive convection (Simeonov and Stern 2008); their role in fingering-driven interleaving is not yet established. In the Faroe Front case, the amplitude ratio was inferred from estimates of cross-front heat and salt fluxes given in section 3d of Hallock (1985). Observational estimation of s is more challenging and has only been done for the Meddy Sharon case. Interleaving growth rates have not yet been measured, but we can say that a valid theory should predict an e-folding time $1/\sigma$ that is not large compared to the time scale on which the front evolves—a few weeks, perhaps. Thus, an interleaving mode with growth rate 10^{-7} s^{-1}, or (116 days)$^{-1}$, would certainly be disrupted by changes in the mean state before attaining large amplitude, whereas a growth rate of 10^{-6} s^{-1}, or (12 days)$^{-1}$, might be expected to result in a measurable interleaving signal.

For these examples, we choose uniform values for the double-diffusive and turbulent diffusivity parameters; that is, the derivatives of the diffusivities appearing in (34) are set to zero. Values of K_S^d, Sc^d, and γ are obtained as in section 2b(2). We do not use the turbulence parameterization described in section 2b(3); instead, the turbulence parameters K_T^t and Pr^t are varied independently while δ is fixed at unity.

a. Effects of K_T^t, Prt: The Meddy Sharon case

We look first at the Meddy Sharon parameter set (column 2 of Table 1, $K_S^d = 2.5 \times 10^{-5}$ m^2 s^{-1}, $\mathrm{Sc}^d = 0.060$, and $\gamma = 0.59$). For this case only, we set $\nu = \kappa_T = \kappa_S = 0$, as the instability is too weak to withstand even molecular mixing. We examine a sequence of cases in which the turbulent diffusivity K_T^t is increased continuously from zero (Fig. 4). The effect of increasing K_T^t from zero is a monotonic decrease in growth rate (Fig. 4a), confirming the stabilizing tendency of ambient turbulence predicted in section 5b. Increasing K_T^t also increases the vertical scale (Fig. 4b).

The turbulent Prandtl number clearly has a major effect on these results. For $\mathrm{Pr}^t = 1$ (Fig. 4a, dotted), instability is quenched for submolecular values of K_T^t. Increasing Pr^t to 20 (solid), we find that interleaving is possible for K_T^t as large as 1.5×10^{-6} m^2 s^{-1}, a small but not uncommon value (Gregg 1998). Thus, the fastest-growing mode is destabilized by increasing turbulent viscosity, as was found previously for modes near the stability boundary (section 5b). There now exists a substantial range of K_T^t in which growth is possible, and the vertical scale is considerably closer to the observed value, 25 ± 5 m, than it is in the absence of turbulence.

The amplitude ratio r is of particular interest because, for baroclinic interleaving in the absence of turbulence, the theoretical value is an order of magnitude larger than the observed value (Smyth 2007). This discrepancy is greater still in the present calculations. In the limit of weak turbulence (Fig. 4c, small values of K_T^t) $r \approx 190$, whereas the Meddy Sharon observations give $r \approx 2$ [the discrepancy with Smyth (2007) is due to our use of the lower value of Sc^d]. With the inclusion of turbulence, however, the predicted amplitude ratio decreases dramatically. At $K_T^t = 10^{-6}$ m^2 s^{-1}, a value characteristic of weak ocean turbulence, the predicted value of r has decreased to 5, a dramatic improvement. Here s agrees well with the observational estimate regardless of the presence of turbulence (Fig. 4d). *These results suggest that inclusion of the effects of ambient turbulence, with the high Prandtl number accounted for, may add significantly to the realism of the classical* (e.g., Stern 1967) *model of interleaving*.

b. Effects of the front width: The Meddy Sharon case

Even with $\mathrm{Pr}^t = 20$, a level of turbulent diffusivity sufficient to yield a realistic vertical scale yields a growth rate that is too small to account plausibly for observations. For example, $K_T^t = 10^{-6}$ m^2 s^{-1} gives $2\pi/\mu \sim 15$ m, which is reasonable, but $\sigma \sim 10^{-8}$ s^{-1}; that is, the e-folding time for growth is several years. This is clearly too slow to account for the growth of intrusions on Meddy Sharon. Likewise, increasing K_T^t to yield a realistic value of r causes the growth rate to drop to implausible levels.

Suppose, however, that the lateral temperature and salinity gradients were actually sharper than the observed values, as would have been true early in the life of the Meddy when interleaving first began to grow. Would it then have been possible for the present linear

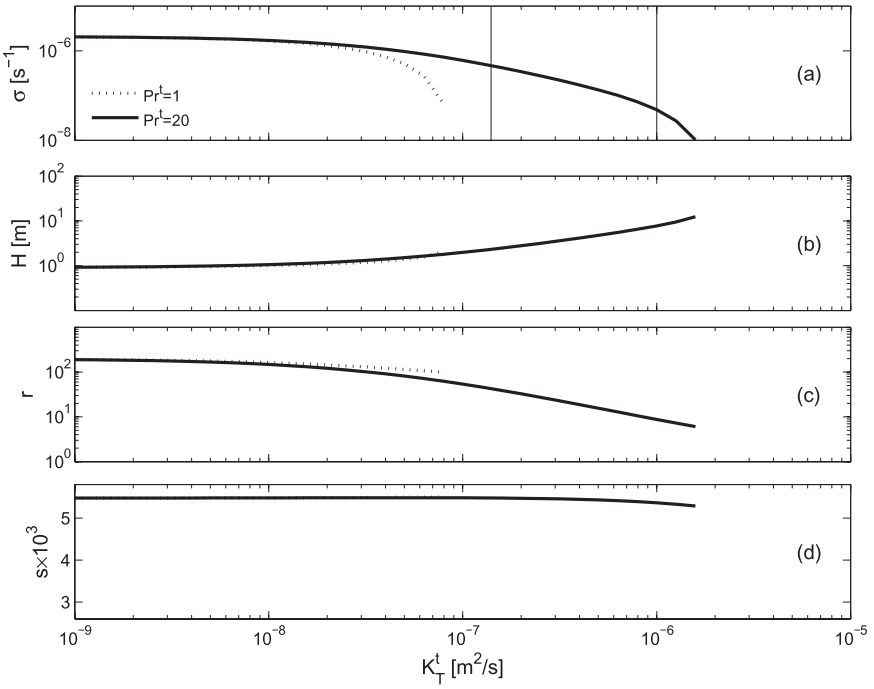

FIG. 4. (a) Growth rate, (b) vertical scale, (c) amplitude ratio, and (d) slope for the fastest-growing mode of thermohaline interleaving as a function of the diffusivity and the Prandtl number characteristic of ambient turbulence. Other parameter values are from observations of the lower flank of Meddy Sharon. Vertical lines on (a) indicate the molecular thermal diffusivity and 10^{-6} m^2 s^{-1}, a value characteristic of weak ocean turbulence (e.g., Peters et al. 1988).

instability to create interleaving layers with the observed scale and a reasonable growth rate? To explore this possibility, we compute the fastest-growing mode for a sequence of cases in which the cross-front gradients of temperature and salinity (and therefore density) were increased by a factor F. For this experiment, the turbulent Prandtl number was set to 20 and the diffusivity was set to the common value 10^{-5} m^2 s^{-1} (Gregg 1998). The molecular viscosity and diffusivities were set to their usual values.

With $F = 1$ there is no instability (Fig. 5a), as we would expect based on the previous subsection. Only a 20% increase in gradients is needed, however, to produce a nonzero growth rate. With the sharpening factor $F = 1.7$, the growth rate reaches 10^{-6} s^{-1}, a reasonable value to account for growth on the evolutionary time scale of a Meddy. The predicted vertical scale is now 14 m (Fig. 5b), a dramatic improvement over the nonturbulent case, though still smaller than the observational estimate 25 ± 5 m. The remaining discrepancy could be partly explained by the tendency of F to decrease as interleaving grows and diffuses the horizontal gradients. As F is decreased below 1.7, the growth rate decreases but the vertical scale increases into the observed range. A related possibility is that the interleaving layers observed on Meddy Sharon had undergone a subharmonic instability, as suggested by Ruddick and Hebert's (1988) observation of a secondary spectral peak with vertical scale near 12 m. In that case the present linear theory would account very well for the observed vertical scale. With $F = 1.7$, $r = 1.6$, and $s = 8 \times 10^{-3}$, both of which are within the observational range. We conclude that, insofar as a 70% decrease in mean gradients over the lifetime of interleaving layers is plausible, the hypothesis that mean gradients associated with observed interleaving layers underestimate the gradients that drove the instability is consistent with observations.

c. *Effects of K_T^t and Pr^t: The Faroe Front case*

We turn next to the Faroe Front observations of Hallock (1985). This front is distinguished from the Meddy Sharon front by a relatively large value of R_ρ, hence weaker double-diffusive processes, and by an isopycnal slope nearly as steep as the isohaline slope, hence a strong influence from baroclinicity. Note that the ratio s_ρ/s_S is approximately equal in all transects (Table 1). This observation is consistent with the hypothesis explored in the previous subsection, namely, that the vertical property gradients were constant while horizontal gradients changed together in response to

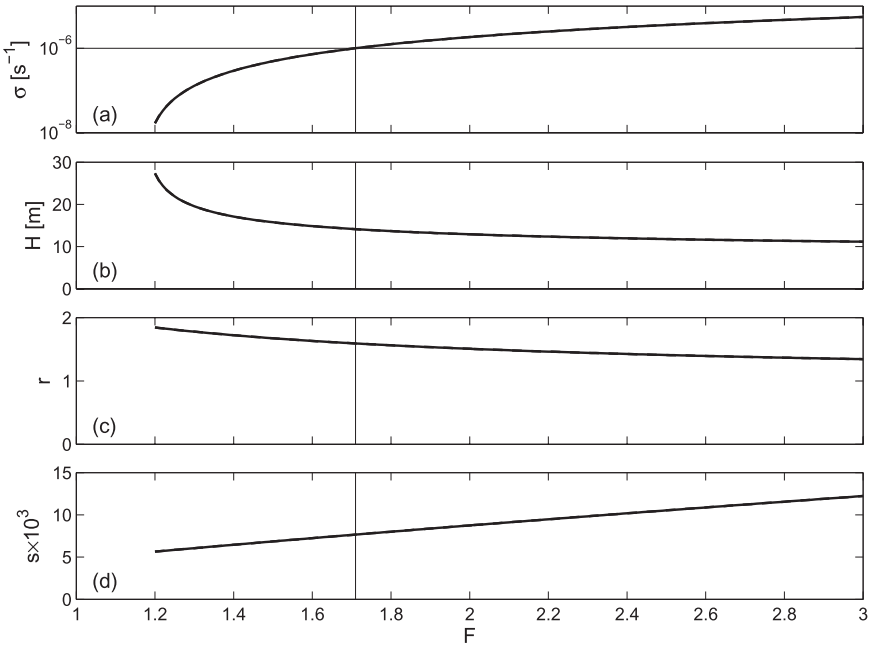

FIG. 5. As in Fig. 4, but as a function of the factor by which isosurface slopes are increased. Other parameter values are from observations of the lower flank of Meddy Sharon.

changes in the width of the front resulting from cross-front mixing and large-scale strain. For this analysis, we choose crossing 2, the case in which the isopycnal and isohaline slopes were steepest. Double-diffusive mixing parameters have the values $K_S^d = 1.07 \times 10^{-5}$ m^2 s^{-1}, $\mathrm{Sc}^d = 0.034$, and $\gamma = 0.55$. As with the Meddy Sharon case, we assume $\delta = 1$ and vary K_T^t and Pr^t independently.

When Pr^t is set to unity, the predicted growth rate drops to zero for even submolecular values of K_T^t (Fig. 6a, dotted curve). With $\mathrm{Pr}^t = 20$ (solid curve), the result is dramatically different. The growth rate *increases* with increasing K_T^t, reaching a maximum at $K_T^t = 10^{-6}$ m^2 s^{-1}, and then declining slightly. This appears to be a manifestation of the McIntyre (1970) instability (cf. section 3b). The geostrophic Richardson number $\tilde{f}^2/s_\rho^2$ is about 3 while the critical Richardson number for $\mathrm{Pr}^t = 20$ is 5.5, so the McIntyre condition for instability is satisfied provided that the isotach slope s_V is less than 0.043. Quantitative correspondence with the McIntyre instability is demonstrated by comparison with the dashed curves in Fig. 6, which show the predictions of (80), (79), and (78). The vertical scale increases in proportion to $K_T^{t1/2}$ as predicted. The interleaving slope is insensitive to K_T^t as in the case of Meddy Sharon and as predicted in the theory. Correspondence with the theory is excellent except at low values of K_T^t, where turbulence is not the dominant mechanism, and at high values, where the expansion parameter k^2 is not $\ll 1$ as assumed.

As in the Meddy Sharon case, the amplitude ratio r takes extreme values when turbulence is weak but decreases to values consistent with observations at higher K_T^t. To match the observed range of vertical scale would require K_T^t to lie in the range $4.6 \times 10^{-5} - 8 \times 10^{-4}$ m^2 s^{-1}. These are very reasonable values for an energetic frontal zone. For this range of K_T^t, we predict $r = 2.8$, a value within error of observations and in dramatic contrast with the nonturbulent value 800.

For this comparison, we have chosen Hallock's (1985) crossing 2, the case in which the frontal gradients were steepest. For this case, instability is predicted even in the presence of strong ambient turbulence, and there is no need to invoke magnified slopes as in the Meddy Sharon case. Had we chosen crossing 5 or the five-transect average, instability would only have been predicted for much smaller values of K_T^t. We could have achieved the same result as for crossing 2 by setting the magnification factor F to 3.0 or 6.7, respectively.

We conclude that the McIntyre mode as described in section 3b accounts very well for the interleaving observed on the Faroe Front by Hallock (1985).

d. *Energetics of the thermohaline and McIntyre modes*

Here we look at interleaving modes from the previous observational examples in light of the energy budget developed in section 2d. In weak turbulence, the modes found on Meddy Sharon exhibit energetics typical of

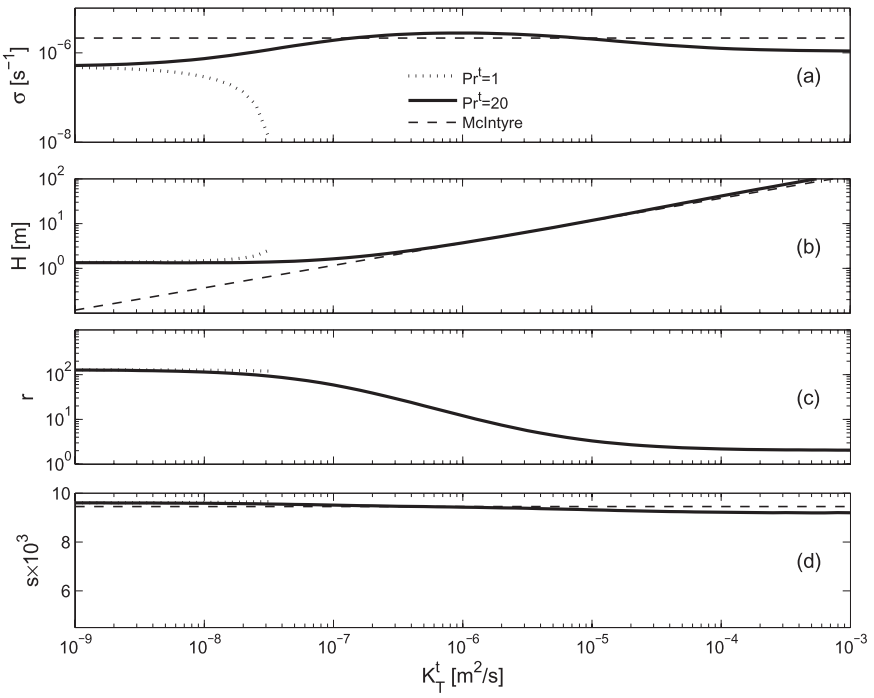

FIG. 6. As in Fig. 4, but as a function of the diffusivity and the Prandtl number characteristic of ambient turbulence. Other parameter values are from observations of the Faroe Front. Dashed curves are parameter values predicted by the McIntyre (1970) theory.

classical thermohaline interleaving (Fig. 7, left side). Kinetic energy growth (Fig. 7a) is driven by a strong buoyancy flux that is counterbalanced by almost equally strong viscous dissipation [these contributions are shown by plusses and circles, respectively, and are defined in (46), (48), and (67)]. Shear production is small (though the larger terms are so closely balanced that a small change in shear production could have a significant effect.) The source of the buoyancy flux that drives the motion is potential energy stored in buoyancy fluctuations (Fig. 7b). This buoyancy variance is generated entirely by salt sheets (asterisks). A small portion of the resulting potential energy is transferred to kinetic energy (plusses). At higher turbulence levels, dissipation (circles) also becomes significant, depleting the buoyancy variance more rapidly than does the transfer to kinetic energy for $K_T^t > 1.5 \times 10^{-8}$ m^2 s^{-1}. As K_T^t exceeds 10^{-6} m^2 s^{-1}, all terms vanish as the mode is stabilized.

We turn next to the energy budgets for the Faroe Front case discussed in section 6c (Fig. 8). A striking difference from the previous case is that both the buoyancy flux term in the kinetic energy equation and the advection term in the buoyancy variance equation (plusses in Figs. 8a,b) are positive. This is because the interleaving slopes lie within the baroclinic wedge and the modes therefore have negative potential energy. As in sloping (or ordinary) convection, gravity feeds both the potential and kinetic energy perturbations.

The energetics are simplest in the limit of strong turbulence (right-hand side of Fig. 8), where the buoyant inputs of both kinetic and potential energy are nearly balanced by turbulent dissipation (circles). The McIntyre mode is therefore energetically similar to sloping convection or baroclinic interleaving. There is also a weak transfer of kinetic energy from the interleaving motions to the mean flow (asterisks on Fig. 8a).

Looking leftward into regimes of weaker turbulence, we see that salt sheets begin to make a contribution to the buoyancy variance. Even in the near-absence of turbulence, though, that contribution is less than one-third of the gravitational component.

e. *Effects of* δ

Differential diffusion appears to have a damping effect on the interleaving structures examined here. For Meddy Sharon, assuming $K_T^t = 10^{-6}$ m^2 s^{-1} and $\mathrm{Pr}^t = 20$, the growth rate at $\delta = 0.7$ is reduced by 25% from the growth rate at $\delta = 1$. In each case, the effect is to damp the fastest-growing mode, contrary to the expansion of the stability boundary predicted in section 5. This result is not unexpected: differential diffusion acts oppositely to salt fingering, in that it transports thermal

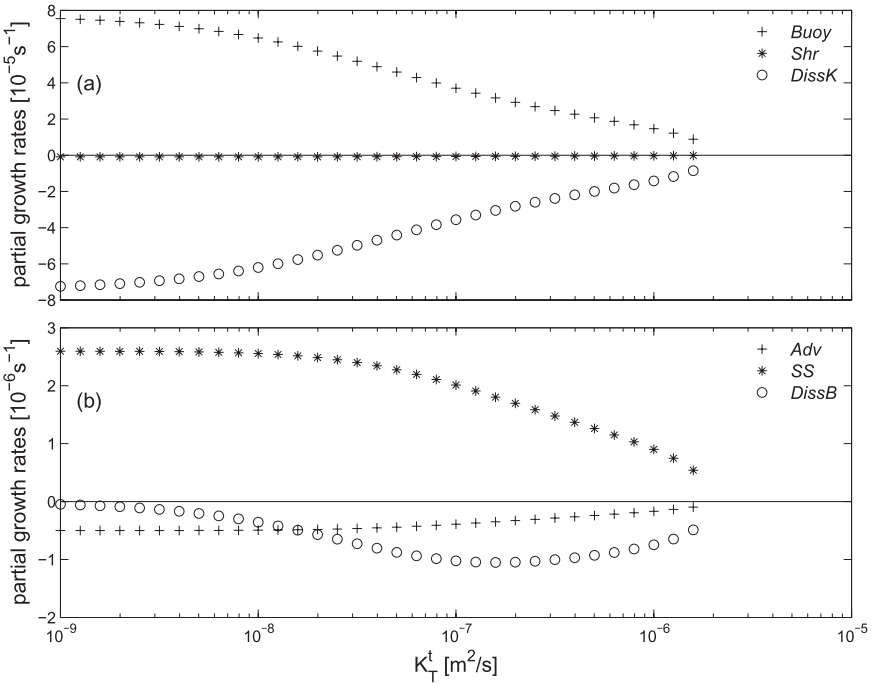

FIG. 7. Budgets for the (a) perturbation kinetic energy and (b) buoyancy variance normalized to give partial growth rates, plotted vs turbulent thermal diffusivities. Parameter values are for Meddy Sharon with $\mathrm{Pr}^t = 20$, corresponding to the thick curves in Fig. 4. Terms are as indicated in the legend and defined in section 2d.

buoyancy more effectively than saline buoyancy. Acting alone, differential diffusion promotes interleaving with slope opposite to that due to salt fingering (sections 2d, 5). We are therefore not surprised to find that interleaving driven mainly by salt fingering is weakened by differential diffusion.

In the case of the Faroe Front, the effect of differential diffusion is slight. Assuming $K_T^t = 10^{-5}$ m^2 s^{-1} and $\mathrm{Pr}^t = 20$, the growth rate at $\delta = 0.7$ is reduced by 3% from the growth rate at $\delta = 1$. We conclude that differential diffusion does not play a role in driving interleaving in these particular regions of parameter space, though it may well be important elsewhere (Hebert 1999; Merryfield 2002).

f. Effects of fluctuations in A and K_T^t: Turbulence-driven interleaving

We return now to the Meddy Sharon parameter set and investigate properties of the fastest-growing instability with turbulence parameters related as in section 2b(3). We begin with a ''control'' calculation (small dots in Fig. 9), in which turbulent diffusivities are spatially uniform as before. Once again, the instability is quenched when the turbulent thermal diffusivity is just under 2×10^{-6} m^2 s^{-1} (the background value $\kappa_b = 10^{-6}$ m^2 s^{-1} has been subtracted for graphical clarity).

Next, we allow the turbulent diffusivities to vary in response to the perturbations [though the salt sheet diffusivities remain uniform; see Walsh and Ruddick (1995) for an analysis of fluctuations in R_ρ]. As shown by the large bullets in Fig. 9, the fluctuations make very little difference in the limit of weak turbulence, but even less turbulence is required to quench the instability than in the case of uniform diffusivities. The growth rate drops to zero at $K_T^t = 1.07 \times 10^{-6}$ m^2 s^{-1} in contrast to $K_T^t = 1.5 \times 10^{-6}$ m^2 s^{-1} in the case of uniform diffusivities. The effects of increasing turbulence on other mode parameters are similar to those seen previously: the vertical scale increases rapidly, the amplitude ratio decreases, and the tilt angle remains approximately constant.

When K_T^t exceeds 1.8×10^{-6} m^2 s^{-1}, an unexpected result is evident. A new mode appears whose properties are distinctly different from the interleaving seen in weaker turbulence. In particular, its growth rate is an order of magnitude greater. Evidently this mode depends on the fluctuations in turbulent diffusivity, as it does not appear when those fluctuations are suppressed (small bullets on Fig. 9). Unlike other modes that depend on diffusivity fluctuations (section 3a), the new mode does not exhibit UV catastrophe; it has a well-defined vertical scale, in this case about 5 m. Its amplitude ratio is

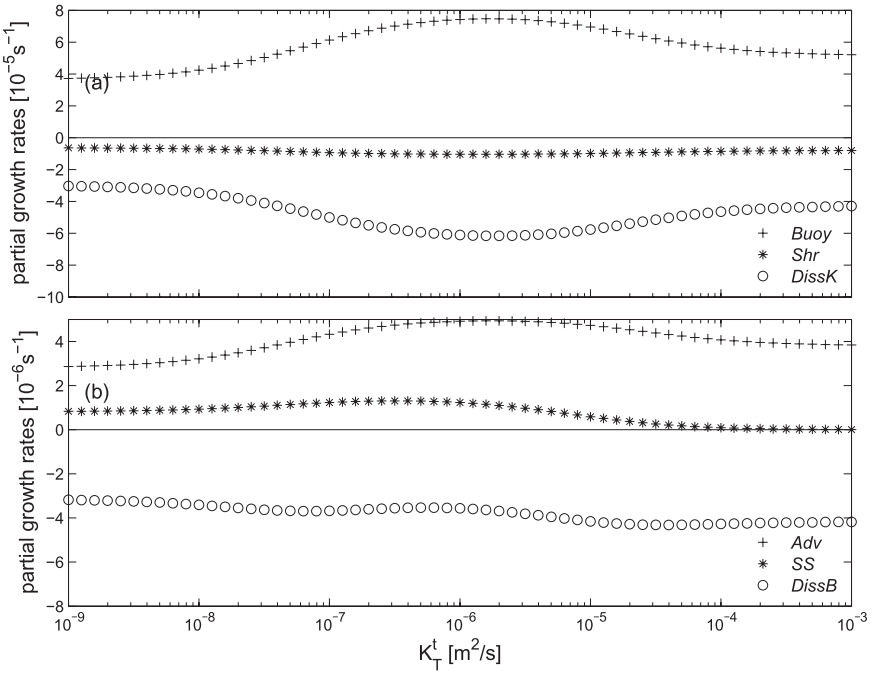

FIG. 8. As in Fig. 7, but for the Faroe Front.

generally $\gg 1$, indicating that buoyancy fluctuations are almost entirely due to temperature. At $K_T^t = 1.5 \times 10^{-6}$ m^2 s^{-1}, the salinity amplitude passes through zero. The intrusion slope s is negative. This mode therefore cannot draw energy from salt stratification or baroclinicity. For $K_T^t > 3 \times 10^{-5}$ m^2 s^{-1} (not shown), the intrusion slope becomes much steeper than the background isosurfaces, and the amplitude ratio decreases to

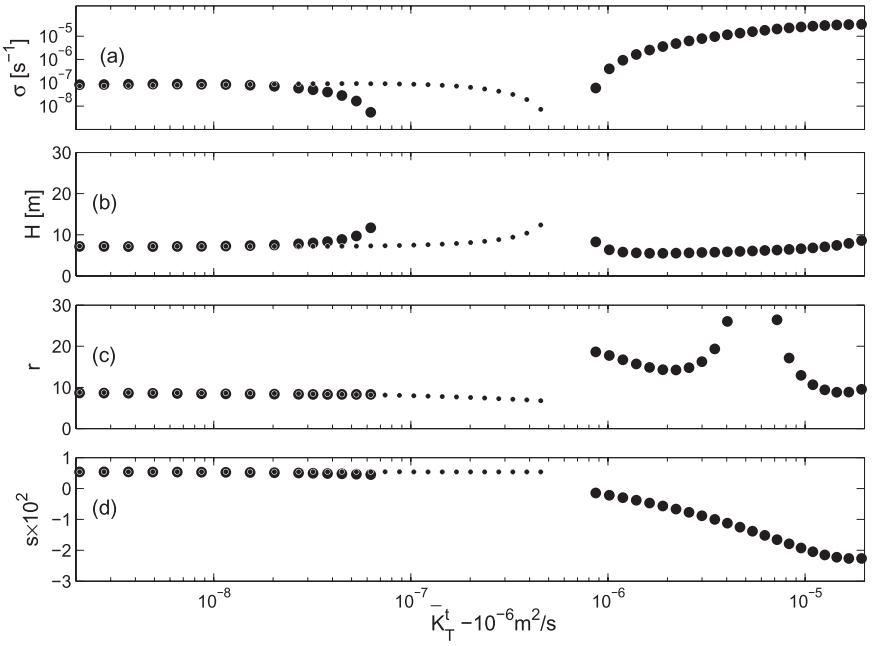

FIG. 9. As in Fig. 4, but as a function of the turbulent thermal diffusivity. Small (large) symbols indicate calculations where fluctuations in K_T^t and A^t due to interleaving were suppressed (retained). The background diffusivity is subtracted for graphical clarity.

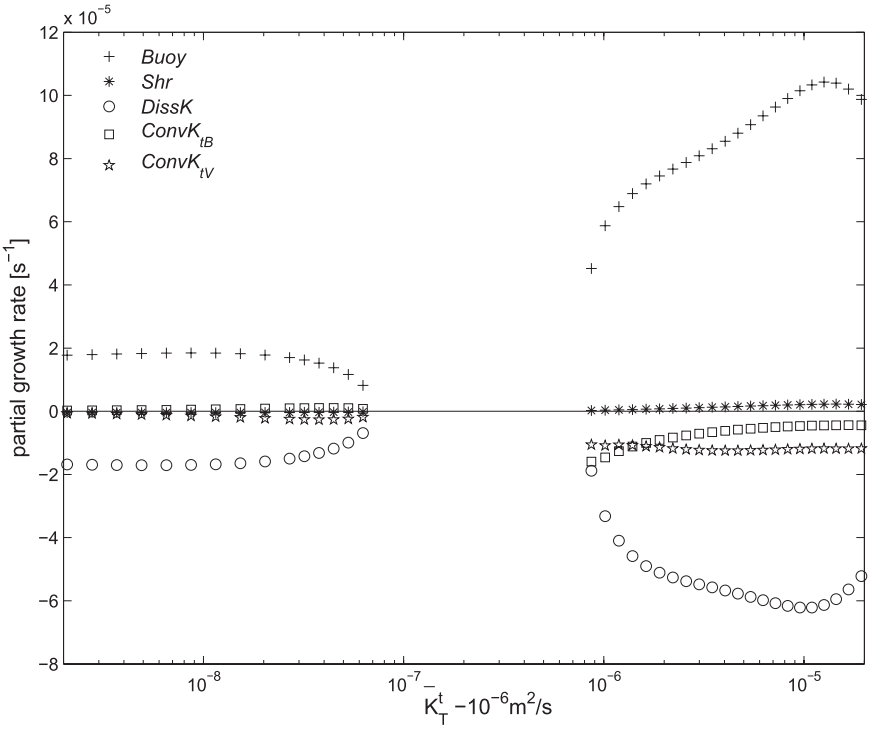

FIG. 10. The perturbation kinetic energy budget normalized to give partial growth rates, plotted vs turbulent thermal diffusivity. Terms are as indicated in the legend and defined in section 2d. The background diffusivity is subtracted for graphical clarity.

the limiting value R_ρ. To learn more about the growth of this mode, we next examine the kinetic energy budget.

Figure 10 shows the kinetic energy budget for the case of fluctuating turbulent diffusivities (large symbols in Fig. 9). For $K_T^t < 1.07 \times 10^{-6}$ m^2 s^{-1}, we have thermohaline interleaving modified by weak turbulence. The motion is driven mainly by buoyancy (plusses) and opposed by the effective viscosity due to double diffusion and turbulence (circles). The new mode driven by turbulent diffusivity fluctuations is evident in the range $K_T^t > 1.08 \times 10^{-6}$ m^2 s^{-1}. Again, the motion is driven by buoyancy and opposed by viscosity. Fluctuations in turbulent viscosity due to perturbations in along-front velocity (stars) and buoyancy (squares) add a significant retarding effect.

While the new mode is driven by buoyancy fluctuations just like thermohaline interleaving, the origin of those buoyancy fluctuations is very different. In the thermohaline regime (Fig. 11, $K_T^t < 1.07 \times 10^{-6}$ m^2 s^{-1}), the buoyancy variance production is driven by the salt sheet term, just as in the weak turbulence limit of Fig. 7; in the turbulent regime ($K_T^t = 1.08 \times 10^{-6}$ m^2 s^{-1}), that term is negative. Instead, buoyancy variance is created by flux convergences due to varying turbulent diffusivities, as described by (65). Convergences are due to both along-front velocity perturbations (B5a, stars) and buoyancy perturbations (B5b, squares). The former are dominant for $K_T^t > 4 \times 10^{-6}$ m^2/s. Besides, being dissipated (circles), the resulting buoyancy variance drives the strong buoyancy flux whose accelerating effect on the intrusions is evident in Fig. 10.

At this stage we know enough about the physics of the new mode of instability seen in Fig. 9 to suggest a mechanism for its growth. Figure 12a is an end-on view of the mean along-front current, with lines indicating the tilt of the isopycnals across the front. Suppose that this mean state is now perturbed by cross-front interleaving motions tilted opposite to the isopycnals (Fig. 12b). The Coriolis effect will turn these motions to the right (we assume the Northern Hemisphere for definiteness), generating the along-front velocity perturbation shown in Fig. 12c. The latter perturbation alternately increases and decreases the thermal wind shear, generating fluctuations in the Richardson number via (28) and hence in the turbulent diffusivity (Fig. 12d). That diffusivity works on the mean buoyancy profile to create a fluctuating downward buoyancy flux (Fig. 12e) whose convergences and divergences generate buoyancy fluctuations (Fig. 12f), which in turn alternately rise and sink under the action of gravity. Because the interleaving slope is

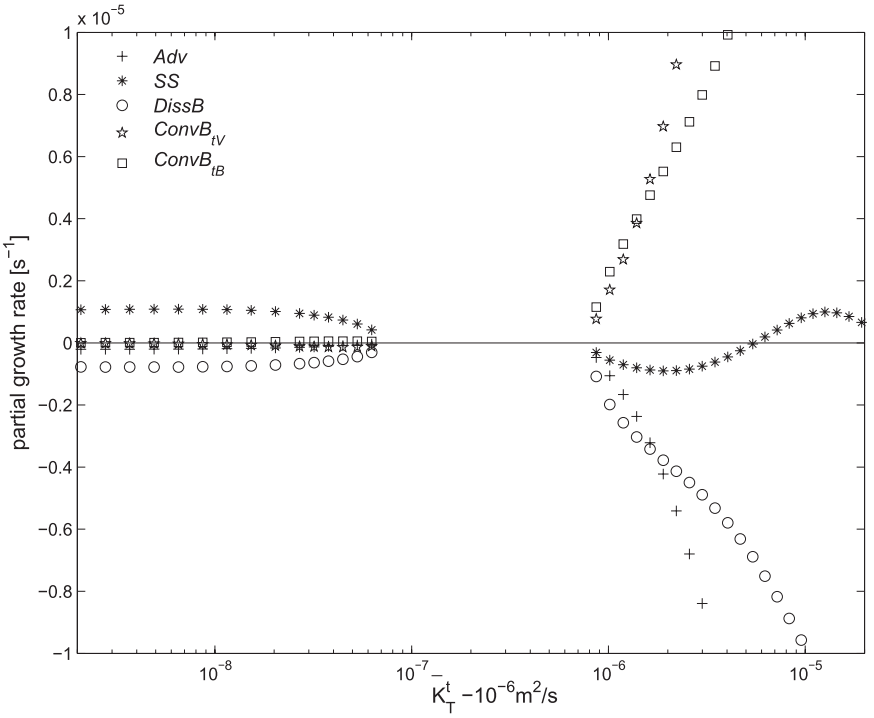

FIG. 11. As in Fig. 10, but for the buoyancy variance budget.

negative, this buoyancy forcing reinforces the along-intrusion velocity perturbation that we postulated originally, creating a positive feedback loop and hence exponential growth. Note that, if s were positive (like the isopycnal slope), then the buoyancy fluctuations shown in (Fig. 12f) would act against the interleaving motions and cause the mode to decay.

A striking characteristic of this instability is its tilt, which is opposite to that of both thermohaline and baroclinic interleaving. This follows from the fact that the buoyancy perturbations are driven primarily by fluctuations in the turbulent flux and are as a result opposite in sign to those driven by the advection of background buoyancy along the intrusions. In interleaving driven by salt sheets and/or baroclinicity, the reverse is true. The mechanism is independent of the double-diffusive process and could therefore occur in any sufficiently turbulent front regardless of the value of R_ρ. The essential prerequisite for the instability is that the decrease in turbulent diffusivity with increasing Richardson number be sufficiently rapid.

The mechanistic picture sketched in Fig. 12 is analogous to Stern's (1967) theory of thermohaline interleaving, in that it retains only those processes most essential for the growth of the mode while neglecting other processes that shape the mode's properties. For example, like the Stern model, this description neglects momentum transport between interleaving layers and therefore does not explain the preferred length scale evident in Fig. 9. A more complete analysis of this and other modes of turbulence-driven interleaving will be pursued separately; for our present purposes, this mechanism plausibly explains the striking tendency of the new mode to tilt opposite to both the isohaline and isopycnal surfaces.

The properties of the turbulence-driven mode are sensitive to the choice of turbulence parameterization. The dynamics admits many different positive feedbacks like that shown in Fig. 12, and plausible changes in parameter values can cause a different mode to become dominant. The instability described here is intended as an example of the rich and largely unexplored class of interleaving mechanisms that result from inhomogeneous turbulence on a baroclinic front.

7. Conclusions

We have explored stationary, normal mode instabilities of a broad, baroclinic front where both double-diffusive and turbulent fluxes are important. We have looked at numerical solutions for particular cases that are relevant to oceanic interleaving regimes, and have also developed a simplified theory that allows us to extend the results continuously across parameter space. Our main conclusions are as follows:

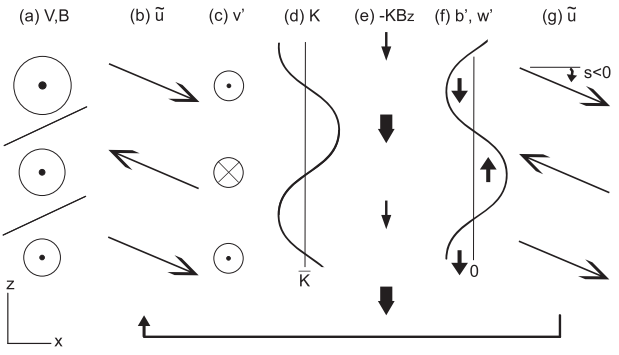

FIG. 12. Proposed mechanism for the low Ri mode shown in Fig. 9. (a) Mean along-front (thermal wind) current. Lines indicate the mean isopycnal slope. (b) Postulated along-intrusion velocity perturbation. (c) Along-front velocity perturbation driven by the Coriolis acceleration acting on (b). (d) Fluctuating turbulent diffusivity caused by perturbations to the thermal wind shear [(a) + (c)]. (e) Downward buoyancy flux driven by fluctuating turbulent diffusivity (d) acting on the mean vertical buoyancy gradient. (f) Buoyancy perturbations driven by the convergences and divergences of the flux (e), and consequent vertical motions. (g) Along-intrusion motions consistent with the vertical motions (f) and a negative intrusion slope. These amplify the postulated perturbation shown in (b), creating a positive feedback loop.

- When ambient turbulence has a Prandtl number greater than unity, turbulent momentum fluxes can compensate for the reduced Schmidt number of salt fingering. In this case, ambient turbulence determines the vertical scale of interleaving.
- An increased turbulent Prandtl number not only induces a preference for the observed large vertical scales, but also increases the growth rate by upsetting the thermal wind like balance of forces that otherwise preserves the equilibrium.
- When turbulence is not accounted for, the thermal–saline amplitude ratio r is 1–2 orders of magnitude larger than observed. Inclusion of turbulence with a high Prandtl number brings r into the observed range.
- In the interleaving structures observed on Meddy Sharon, the property gradients are insufficient to predict interleaving growth, even when improved turbulence models are used. We suggest that this is due to the effectiveness of interleaving in erasing those property gradients. As is often true with instabilities, the observation of a finite-amplitude disturbance indicates that the adjustment back to a stable state is underway or even complete, so that measurements of mean gradients underestimate the gradients that drove the instability originally.
- The Faroe Front is an example of a baroclinic front where interleaving is likely due to the McIntyre (1970) instability.
- We have identified a new mode of interleaving instability driven by the sensitivity of turbulence to fluctuations in the Richardson number. This mode can in theory grow on any baroclinic front, provided turbulence is strong enough, and ''strong enough'' means only, in this case, that $K_T^t = 1.8 \times 10^{-6}$ m^2 s^{-1}, a value smaller than the typical value for the thermocline. The mechanism involves the reverse diffusion process described in section 3a, acting in concert with the Coriolis acceleration. It exhibits a well-defined vertical scale and a tilt angle opposite to (and stronger than) that predicted for interleaving driven by salt sheets or baroclinicity. Further theoretical study is needed to establish measureable characteristics of this mode that could facilitate observational verification.

The layering instabilities of Phillips (1972) and Posmentier (1977) have been studied extensively, but their interaction with other mechanisms in a frontal environment creates a rich physics we have barely begun to explore. The mechanism described in Fig. 12 is only one of many possible new instabilities.

Shcherbina et al. (2009) have drawn a useful distinction between ''active'' and ''passive'' mechanisms for interleaving. In the former, the interleaving motions organize the local property gradients so as to amplify their own growth; in the latter, interleaving results from passive advection by motions due to unrelated causes, such as mesoscale turbulence. Active mechanisms have included both flavors of double diffusion as well as differential diffusion and inertial instability. To this list we now add the new class of interleaving driven by turbulence and suggest that it may explain some observations that do not fit previous active mechanisms and would otherwise be assumed to be passive.

Our focus here has been entirely on $R_\rho > 1$, that is, fingering-favorable stratification. The turbulence-driven mode described in section 6f may be even more important in diffusive convection $0 < R_\rho < 1$ or differential diffusion ($R_\rho < 0$) regimes, where its interleaving slope can match those of the interleaving mechanisms already known. The resulting positive feedbacks could lead to powerful new modes of interleaving instability.

Because of the crucial role ambient turbulence plays, future theoretical studies of interleaving should represent ambient turbulence using models at least as realistic as those used here. Instabilities driven directly by turbulence are likely to be represented best by one-dimensional, second-order closure models (e.g., Burchard and Petersen 1999; Canuto et al. 2008). Extension to the

finite-amplitude regime, as in Walsh and Ruddick (1998) and Mueller et al. (2007), is also essential. This theoretical progress must be accompanied by new observational work on baroclinic fronts. Observational strategies should allow for estimation of small-scale diffusivities as well as mean vertical and cross-front gradients of temperature, salinity and alongfront velocity, vertical scales, tilt angles, and amplitudes (including velocity).

Acknowledgments. Everything in this paper follows from the pioneering insights of the late Melvin Stern. The paper has also benefited from the comments of two anonymous reviewers. Funding was provided by the National Science Foundation under Grant OCE0622922.

REFERENCES

Armi, L., D. Hebert, N. Oakey, J. Price, P. Richardson, H. Rossby, and B. Ruddick, 1989: Two years in the life of a Mediterranean salt lens. *J. Phys. Oceanogr.,* **19,** 354–370.

Burchard, H., and O. Petersen, 1999: Models of turbulence in the marine environment—A comparative study of two-equation turbulence models. *J. Mar. Syst.,* **21,** 29–53.

Canuto, V. M., Y. Cheng, and A. M. Howard, 2008: A new model for Double Diffusion + Turbulence. *Geophys. Res. Lett.,* **35,** L02613, doi:10.1029/2007GL032580.

Esau, I. N., and A. A. Grachev, 2007: Turbulent Prandtl Number in Stably Stratified Atmospheric Boundary Layer: Intercomparison between LES and SHEBA Data. *e-WindEng. J.,* **5.** [Available online at http://ejournal.windeng.net.]

Galperin, B., S. Sukoriansky, and P. Anderson, 2007: On the critical Richardson number in stably stratified turbulence. *Atmos. Sci. Lett.,* **8,** 65–69.

Gargett, A., 2003: Differential diffusion: An oceanographic primer. *Prog. Oceanogr.,* **56,** 559–570.

Gregg, M., 1987: Diapycnal mixing in the thermocline: A review. *J. Geophys. Res.,* **92** (C5), 5249–5286.

——, 1998: Estimation and geography of diapycnal mixing in the stratified ocean. *Physical Processes in Lakes and Oceans,* J. Imberger, Ed., Coastal Estuarine Series, Vol. 54, Amer. Geophys. Union, 305–338.

Hallock, Z., 1985: Variability of frontal structure in the southern Norwegian Sea. *J. Phys. Oceanogr.,* **15,** 1245–1254.

Hazel, P., 1972: Numerical studies of the stability of inviscid parallel shear flows. *J. Fluid Mech.,* **51,** 39–62.

Hebert, D., 1999: Intrusions: What drives them? *J. Phys. Oceanogr.,* **29,** 1382–1391.

——, and B. R. Ruddick, 2003: Differential mixing by breaking internal waves. *Geophys. Res. Lett.,* **30,** 1042, doi:10.1029/2002GL016250.

Holyer, J., 1983: Double diffusive interleaving due to horizontal gradients. *J. Fluid Mech.,* **137,** 347–362.

——, T. Jones, M. Priestly, and N. Williams, 1987: The effect of vertical temperature and salinity gradients on double diffusive interleaving. *Deep-Sea Res.,* **34,** 517–530.

Huppert, H. E., 1971: On the stability of a series of double-diffusive layers. *Deep-Sea Res.,* **18,** 1005–1021.

Jackson, P., and C. Rehmann, 2003: Laboratory measurements of differential diffusion in a diffusively stable, turbulent flow. *J. Phys. Oceanogr.,* **33,** 1592–1603.

Kimura, S., and W. Smyth, 2007: Direct numerical simulations of salt sheets and turbulence in a double-diffusive shear layer. *Geophys. Res. Lett.,* **34,** L21610, doi:10.1029/2007GL031935.

Kuzmina, N., and V. Rodionov, 1992: Influence of baroclinicity on formation of thermohaline intrusions in ocean frontal zones. *Izv. Acad. Sci. USSR, Atmos. Oceanic Phys.,* **28,** 804–810.

——, and V. Zhurbas, 2000: Effects of double diffusion and turbulence on interleaving at baroclinic ocean fronts. *J. Phys. Oceanogr.,* **30,** 3025–3038.

Large, W., J. McWilliams, and S. Doney, 1994: Ocean vertical mixing: A review and a model with a nonlocal boundary layer parameterization. *Rev. Geophys.,* **32,** 363–403.

Linden, P., 1974: Salt fingers in a steady shear flow. *Geophys. Fluid Dyn.,* **6,** 1–27.

May, B., and D. Kelley, 1997: Effect of baroclinicity on double-diffusive interleaving. *J. Phys. Oceanogr.,* **27,** 1997–2008.

——, and ——, 2002: Contrasting the interleaving in two baroclinic ocean fronts. *Dyn. Atmos. Oceans,* **36,** 23–42.

McIntyre, M., 1970: Diffusive destabilization of the baroclinic circular vortex. *Geophys. Fluid Dyn.,* **1,** 19–57.

Merryfield, W., 2002: Intrusions in double-diffusively stable Arctic waters: Evidence for differential mixing? *J. Phys. Oceanogr.,* **32,** 1452–1459.

Mueller, R. D., W. D. Smyth, and B. R. Ruddick, 2007: Shear and convective turbulence in a model of thermohaline intrusions. *J. Phys. Oceanogr.,* **37,** 2534–2549.

Pacanowski, R., and S. Philander, 1981: Parameterization of vertical mixing in numerical models of tropical oceans. *J. Phys. Oceanogr.,* **11,** 1443–1451.

Peters, H., M. Gregg, and J. O'Toole, 1988: On the parameterization of equatorial turbulence. *J. Geophys. Res.,* **93,** 1199–1218.

Phillips, O., 1972: Turbulence in a strongly stratified fluid: Is it unstable? *Deep-Sea Res.,* **19,** 79–81.

Posmentier, E., 1977: The generation of salinity finestructure by vertical diffusion. *J. Phys. Oceanogr.,* **7,** 298–300.

Radko, T., 2003: A mechanism for layer formation in a double-diffusive fluid. *J. Fluid Mech.,* **497,** 365–380.

Ruddick, B., 1992: Intrusive mixing in a Mediterranean salt lens: Intrusion slopes and dynamic mechanisms. *J. Phys. Oceanogr.,* **22,** 1274–1285.

——, and D. Hebert, 1988: The mixing of Meddy "Sharon." *Small-Scale Turbulence and Mixing in the Ocean,* J. Nihoul and B. Jamart, Eds., Oceanography Series, Vol. 46, Elsevier, 249–261.

——, and O. Kerr, 2003: Oceanic thermohaline intrusions: Theory. *Prog. Oceanogr.,* **56,** 483–497.

——, and K. Richards, 2003: Oceanic thermohaline intrusions: Observations. *Prog. Oceanogr.,* **56,** 499–527.

——, T. McDougall, and J. Turner, 1989: The formation of layers in a uniformly stirred density gradient. *Deep-Sea Res.,* **36,** 579–609.

Shcherbina, A. Y., M. C. Gregg, M. H. Alford, and R. R. Harcourt, 2009: Characterizing thermohaline intrusions in the North Pacific subtropical frontal zone. *J. Phys. Oceanogr.,* **39,** 2735–2756.

Simeonov, J., and M. Stern, 2008: Double-diffusive intrusions in a stable salinity gradient "heated from below." *J. Phys. Oceanogr.,* **38,** 2271–2282.

Smyth, W., 2007: Instabilities of a baroclinic, double diffusive frontal zone. *J. Phys. Oceanogr.,* **38,** 840–861.

——, and J. McWilliams, 1998: Instability of an axisymmetric vortex in a stably stratified, rotating environment. *Theor. Comput. Fluid Dyn.,* **11,** 305–322.

——, and S. Kimura, 2007: Instability and diapycnal momentum transport in a double-diffusive stratified shear layer. *J. Phys. Oceanogr.,* **37,** 1551–1565.

——, J. Moum, and D. Caldwell, 2001: The efficiency of mixing in turbulent patches: Inferences from direct simulations and microstructure observations. *J. Phys. Oceanogr.,* **31,** 1969–1992.

——, J. Nash, and J. Moum, 2005: Differential diffusion in breaking Kelvin–Helmholtz billows. *J. Phys. Oceanogr.,* **35,** 1004–1022.

Stern, M., 1967: Lateral mixing of water masses. *Deep-Sea Res.,* **14,** 747–753.

——, 1975: *Ocean Circulation Physics*. International Geophysics Series, Vol. 19, Academic Press, 246 pp.

——, T. Radko, and J. Simeonov, 2001: Salt fingers in an unbounded thermocline. *J. Mar. Res.,* **59,** 355–390.

St. Laurent, L., and R. Schmitt, 1999: The contribution of salt fingers to vertical mixing in the North Atlantic Tracer Release Experiment. *J. Phys. Oceanogr.,* **29,** 1404–1424.

Toole, J., and D. Georgi, 1981: On the dynamics of double-diffusively driven intrusions. *Prog. Oceanogr.,* **10,** 123–145.

Walsh, D., and B. Ruddick, 1995: Double-diffusive interleaving: The influence of nonconstant diffusivities. *J. Phys. Oceanogr.,* **25,** 348–358.

——, and ——, 1998: Nonlinear equilibration of thermohaline intrusions. *J. Phys. Oceanogr.,* **28,** 1043–1069.

——, and ——, 2000: Double-diffusive interleaving in the presence of turbulence: The effect of a nonconstant flux ratio. *J. Phys. Oceanogr.,* **30,** 2231–2245.

Zaron, E., and J. Moum, 2009: A new look at Richardson number mixing schemes for equatorial ocean modeling. *J. Phys. Oceanogr.,* **39,** 2652–2664.

Zhang, J., R. Schmitt, and R. Huang, 1998: Sensitivity of the GFDL modular ocean model to parameterization of double-diffusive processes. *J. Phys. Oceanogr.,* **28,** 589–605.

Zhurbas, V., and I. Oh, 2001: Can turbulence suppress double-diffusively driven interleaving completely? *J. Phys. Oceanogr.,* **31,** 2251–2254.

——, N. Kuzmina, and I. Lozovatskiy, 1988: The role of baroclinicity in intrusive layering in the ocean. *Oceanology,* **28,** 34–36.